ANTIOXIDANTS & REDOX SIGNALING
Volume 17, Number 9, 2012

DOI: 10.1089/ars.2012.4564

FORUM REVIEW ARTICLE

How Do Heme-Protein Sensors Exclude Oxygen? Lessons Learned from Cytochrome c′, *Nostoc puntiforme* Heme Nitric Oxide/Oxygen-Binding Domain, and Soluble Guanylyl Cyclase

Ah-lim Tsai,[1] Emil Martin,[2] Vladimir Berka,[1] and John S. Olson[3]

Abstract

Significance: Ligand selectivity for dioxygen (O_2), carbon monoxide (CO), and nitric oxide (NO) is critical for signal transduction and is tailored specifically for each heme-protein sensor. Key NO sensors, such as soluble guanylyl cyclase (sGC), specifically recognized low levels of NO and achieve a total O_2 exclusion. Several mechanisms have been proposed to explain the O_2 insensitivity, including lack of a hydrogen bond donor and negative electrostatic fields to selectively destabilize bound O_2, distal steric hindrance of all bound ligands to the heme iron, and restriction of in-plane movements of the iron atom. ***Recent Advances:*** Crystallographic structures of the gas sensors, *Thermoanaerobacter tengcongensis* heme-nitric oxide/oxygen-binding domain (*Tt* H-NOX[1]) or *Nostoc puntiforme* (*Ns*) H-NOX, and measurements of O_2 binding to site-specific mutants of *Tt* H-NOX and the truncated β subunit of sGC suggest the need for a H-bonding donor to facilitate O_2 binding. ***Critical Issues:*** However, the O_2 insensitivity of full length sGC with a site-specific replacement of isoleucine by a tyrosine on residue 145 and the very slow autooxidation of *Ns* H-NOX and cytochrome c′ suggest that more complex mechanisms have evolved to exclude O_2 but retain high affinity NO binding. A combined graphical analysis of ligand binding data for libraries of heme sensors, globins, and model heme shows that the NO sensors dramatically inhibit the formation of six-coordinated NO, CO, and O_2 complexes by direct distal steric hindrance (cyt c′), proximal constraints of in-plane iron movement (sGC), or combinations of both following a sliding scale rule. High affinity NO binding in H-NOX proteins is achieved by multiple NO binding steps that produce a high affinity five-coordinate NO complex, a mechanism that also prevents NO dioxygenation. ***Future Directions:*** Knowledge advanced by further extensive test of this "sliding scale rule" hypothesis should be valuable in guiding novel designs for heme based sensors. *Antioxid. Redox Signal*. 17, 1246–1263.

Introduction

A LARGE NUMBER of heme protein-based sensors for nitric oxide (NO), carbon monoxide (CO), and dioxygen (O_2) have been characterized in the last two decades. These heme proteins include over 50 sensor proteins exhibiting four different types of heme-binding motifs: heme-binding PER-ARNT-SIM (or PAS), globin-coupled sensor, CooA, and heme-NO-binding domains (39, 97). Some outstanding examples are the FixL, EcDos, HemAT, CooA, cytochrome c′ (cyt c′), several Heme-NO/OXygen binding domain proteins (or H-NOXs) (8, 15, 63, 81, 87, 117, 130), and soluble guanylyl cyclase (sGC) (44, 54, 66, 78, 91, 119). sGC catalyzes the formation of cyclic GMP from GTP and is the only known heme-containing enzyme that is intensely activated by NO (44, 54, 66, 78, 91, 119). NO binds to the heme prosthetic group to generate an equilibrium five-coordinate low-spin NO complex with dissociation of the proximal histidine ligand. NO binding leads to >100-fold activation of cyclase activity. CO also binds to sGC but forms a six-coordinate heme complex, and, in the absence of other effector molecules, only causes a minor increase in enzyme activity (106). The most striking phenomenon is that sGC is isolated as a stable 5c-ferrous hemeprotein. There is no O_2 binding in 100% O_2-saturated buffer and very little autooxidation occurs, even when the protein is left in air at room temperature for several days (113).

Divisions of [1]Hematology and [2]Cardiology, Department of Internal Medicine, University of Texas Health Science Center at Houston, Houston, Texas.
[3]Department of Biochemistry and Cell Biology and W.M. Keck Center for Computational Biology, Rice University, Houston, Texas.

Similarly, cytochrome c′ and other H-NOX proteins either exclude or show little O_2 binding (49, 81, 122). How sGC and other heme sensors achieve O_2 exclusion, inhibition of autooxidation, and high NO affinity is the theme of this review article.

Intrinsic Ligand Selectivity of Heme

Heme, by itself, shows a wide range of reactivity with diatomic gases, anions, and bases. The anionic ligands, azide, cyanide, nitrite, thiocyanate, and halides only bind to hemin (Fe(III)-protoporphyrin IX), which has a net +1 charge at the heme core. On the other hand, the Lewis bases with nonbonded electron pairs, including the diatomic gases NO, CO, and O_2, tend to coordinate primarily with heme (Fe(II)-protoporporphyrin IX) (120). The prominent interaction in this case is not charge but backbonding between the metal d orbitals (93) and the two ligand π antibonding (π^*) orbitals. CO has two empty degenerate π^* orbitals (LUMO), NO has one electron in these two π^* orbitals (HOMO), and O_2 has both π^* orbitals occupied (as triplet O_2) (61, 72). Model hemes differentially bind NO, CO, and O_2, which are separated by 1 electron in their outer shell, 10–12 electrons, respectively. The binding affinities are in the order NO > > CO > > O_2. In the case of O_2, there is little back-bonding capability with filled π^* orbitals, and as a result, O_2 dissociation rate constants are normally several orders of magnitude greater than those for CO and NO (Table 1).

The free radical nature of NO causes it to have the highest reactivity with iron and, therefore, the highest bimolecular association rate constants, which normally represent the rate of ligand movement into the protein active site (33, 83, 104). NO is also able to react with both the ferric and ferrous forms of all heme proteins (110). The Fe(II)-NO complex exhibits geometric flexibility (24). Normally, a linear conformation (sp hybridization) is observed for the ferric complex, where NO has triple bond character, and a bent conformation (sp2 hybridization) is observed for the ferrous complex, where the bound NO has a double bond character. However in both cases, the molecular orbital pattern is on the borderline between linear and bent geometries according to the general rule developed by Feltham and Enemark for $\{MNO\}^n$, where n is the sum of the metal d-electrons and the NO π^* electrons (31). The M-N-O conformation is predicted to be linear for $n \leq 6$, but bent for $n > 6$. For the Fe(III)NO and Fe(II)NO, n equals 6 and 7, respectively. Thus any change in redox state of the iron or steric hindrance and electrostatic interactions with the bound NO may easily change the ligand conformation. For the same transition metal series, NO ligated to Mn(II)PPIX, $n = 6$, should be linear, whereas NO coordinated to Co(II)PPIX, $n = 8$, should be bent. Because it is a 3-electron donor, NO is a strong field ligand, and both the six-coordinate and five-coordinate NO heme complexes are low-spin due to large energy splitting between the t_{2g} and e_g d orbitals (72). In contrast to FeNO, FeCO always assumes an almost linear geometry, Fe-C-O ~180°, and O_2 always shows a bent conformation, Fe-O-O ~110°–120° (92, 93, 103, 125).

Effect of Protein on Heme Ligand Selectivity

Although the intrinsic geometries of model heme-gas complexes remain relatively unchanged in proteins, the relative affinities for NO, CO, and O_2 binding can be altered dramatically when the heme is associated with protein. The chemical nature and geometry of the axial ligand provided by the protein on the proximal side of the heme group can alter the absolute reactivity of the iron atom over several orders of magnitude (47, 84). Steric constraints and electrostatic interaction with the bound ligand on the distal side of the heme group can dramatically influence ligand selectivity (84, 90). Different stereochemical strategies appear to have evolved to optimize both absolute ligand affinity and selectivity between NO, CO, and O_2 and to meet specific physiological needs for O_2 storage and transport [*e.g.*, myoglobin (Mb), hemoglobin (Hb) (109)], O_2 sensing (*e.g.*, FixL, EcDos, HemAT) (39), NO storage/transport (nitrophorins) (126), NO sensing (*e.g.*, sGC, cyt c′, and other sensors of NO) (15, 22, 26), and CO sensing (*e.g.*, CooA and NPAS in circadian rhythm control) (8, 29, 95).

For example, the affinity of CO for model heme with a proximal imidazole base is roughly 4000 times greater than that for O_2, whereas in mammalian Mbs and Hbs the ratio K_{CO}/K_{O2} is only 25–200, indicating a selective increase in affinity for O_2 in the globins (84) (Table 1). In these proteins, the highly conserved distal E7 histidine donates a strong hydrogen bond to preferentially stabilize bound O_2 by a factor of roughly 1000 (84, 90). Direct steric hindrance from protein residues on the bound ligands, although greatly affecting absolute affinity, causes little (≤2–3-fold) additional discrimination between NO, CO, and O_2.

Nitrophorins are NO storage hemeproteins present in the saliva of the blood-sucking insect *Rhodnius proxlixus* and achieve complete selectivity for NO by keeping the iron atom oxidized and incapable of binding O_2 and CO (126). When the uncharged NO binds to the hemin iron atom, it displaces water molecules from the distal portion of the heme pocket and induces movement of two flexible loops to close the active site by a mechanism referred to as a hydrophobic trap. These conformational changes due to NO binding are in sharp contrast to the lack of structural alterations when anionic ligands, such as cyanide, bind to nitrophorin (127).

Hemeproteins involved in sensing diatomic gases are typical sensor/effector two-component systems (39). For some of these proteins, functional selectivity does not occur directly during the ligand binding step but instead occurs during coupling with the effector or enzymatic domain. For example, the O_2 sensor FixL from nitrogen fixing *Rhizobia* has an N-terminal heme domain and a histidine kinase C-terminal domain (74). In this protein, the partial negative charge on bound O_2 attracts a key basic residue, Arg220, to move toward the center of the porphyrin (10). This movement of Arg220 is believed to be the conformational switch that leads to signal transduction and activation of the histidine kinase in FixL. Although NO and CO also bind well to ferrous FixL, the resultant neutral FeNO and FeCO complexes fail to induce the required Arg220 conformational change and the kinase domain remains inactive (1, 10).

CooA is a CO sensor/transcription factor found in *Rhodospirillum rubrum* and represents another case where activation of the nonheme domain is ligand specific. This protein has a heme regulatory N-terminal domain and a C-terminal DNA-binding domain (95). Reduction of the heme iron center causes a proximal ligand shift from a Cys thiolate (Fe^{+3}) to a His imidazole (Fe^{+2}) (9). CO only binds to the reduced heme and thus greatly increases the reduction potential of the iron atom. The concomitant proximal ligand shift causes a large movement of

Table 1. Gaseous Ligand Binding Parameter Values for sGC, $\alpha\beta$I145YsGC, Cytochrome c', NS H-NOX, Mb, H64V Mb, Lb, H61L Lb and Heme Model

Sample	K_D (M)	k_{off}, (s^{-1})	k_{on}, ($\mu M^{-1}s^{-1}$)	*Ref. and* comments[a]
Wild type sGC:				
NO	4.2×10^{-12}[b], 5.4×10^{-8}[c]	0.0006, 27[c] ~50	140, 480[c] 0.24, 1.0	(114, 131), 4°C, (68) (131), 4°C, (68)
CO	2.6×10^{-4}	10.7	0.04	(13, 68, 112)
O_2	1–3 (predicted)	N/A	N/A	(13)
Cytc':				
NO	$1.2\times10^{-6}/1.4\times10^{-7}$	0.006	0.044	(2, 36, 37)
CO	2.8×10^{-4}	0.028	0.00010	(6, 49)
O_2	~1–10 (predicted)	~5000 (predicted)	~5000 (predicted)	
L16A Cytc':				
NO	7.0×10^{-14}	2×10^{-7}	2.9	(36)
CO	3.7×10^{-12}	0.0000037	1.0	(6)
O_2	4.9×10^{-8}	0.17	3.5	(36)
$\alpha\beta$I145Y sGC:				
NO	$\leq0.8\times10^{-6}$	≤10	12	(68)
CO	2.5×10^{-4}	0.8	0.003	(68)
O_2	N/A	N/A	N/A	(68)
NS H-NOX:				
NO	1.7×10^{-10}	0.05	300	1st 6C-NO complex (122)
	0.8×10^{-6}	1.9	2.4	2nd 6C-NO complex (122)
CO	1.4×10^{-6}	3.6	3.0	6C-NO complex (122)
O_2	1.3×10^{-2}[d] $1–2\times10^{-2}$ (predicted)	N/A	N/A	Slow autooxidation (122)
Mb(II), whale:				
NO	4.5×10^{-12}	0.0001	22	(30, 93)
CO	3.7×10^{-8}	0.019	0.51	(18, 93)
O_2	0.9×10^{-6} ~1×10^{-4} (predicted)	15	17	(18, 93)
H64V Mb:				
NO	4.0×10^{-12}	0.0011	270	(84, 93)
CO	6.8×10^{-9}	0.048	7.0	(84, 93)
O_2	9.1×10^{-5} ~7×10^{-5} (predicted)	10,000	110	(84, 93)
Lb(II), soybean:				
NO	1.1×10^{-13}	0.00002	190	(41)
CO	5.6×10^{-10}	0.0084	15	(41)
O_2	4.3×10^{-8}	5.6	130	(41)
H61LLb:				
NO	6.25×10^{-14}	0.00002	320	(41)
CO	1.4×10^{-11}	0.0024	170	(41)
O_2	5.9×10^{-8}	24	400	(41)
Fe(II)PP(1-MeIm):				
NO	1.6×10^{-12}	0.00029	180	(42, 99)
CO	1.3×10^{-9}	0.0023	1.8	(42, 99)
O_2	0.6×10^{-5} ~1×10^{-5} (predicted)	310	55	(20)

[a]Unless otherwise specified, the experimental temperature was 20°C–25°C.
[b]Calculated as k_{off}/k_{on} using values from refs. (51, 131).
[c]Calculated based on the k_{off} and k_{on} for 6c-NO complex determined in this study at 24°C.
[d]Determined by O_2 binding isotherm under high pressure (132).
N/A, not applicable; N/D, not determined.

the C-helix and leads to a conformational change in the DNA binding domain. Thus, signaling in CooA involves both a redox and a conformational switch (7, 8). O_2 does appear to bind CooA, but very quickly oxidizes the iron atom and thus cannot sustain the conformation required for affecting DNA binding (7, 96). NO binding to CooA results in a 5c-NO-heme complex with a very different protein conformation that is not competent for activating the conformational switch (94).

EcDos is an O_2 sensor found in *Escherichia coli* and has an N-terminal PAS heme domain and a phosphodiesterase C-terminal domain (39). Reduction of the ferric form of this enzyme causes binding of a Met side chain to form a

hexacoordinate heme complex, which in turn causes a scissor-like motion in the quaternary structure of the EcDos homodimer (58). This conformational change leads to the association of the phosphodiesterase domains to form an active enzyme (58). O_2 and CO bind to ferrous EcDos with a similar affinity ($K_D \sim 10\,\mu M$) and both displace the bound Met side chain, inactivating the enzyme. The association rate constants for all three diatomic gases (O_2, CO, and NO) are very low, $\leq 0.003\,\mu M^{-1}s^{-1}$ (40). Thus, signal transduction, at least for O_2 and CO, is determined by the natural abundance of individual gaseous ligand, which in the case of O_2 is high enough to inactivate the enzyme under aerobic conditions.

sGC: A Highly Selective NO Receptor

The signaling mechanisms described for FixL, CooA, and EcDos and the NO storage and delivery mechanisms of nitrophorin all have structural support from crystallographic data. No crystal structure has been determined for sGC, and as a result, mechanistic information regarding signal transduction in this enzyme relies on spectroscopic and kinetic studies of wild-type and mutant proteins. In contrast to the gas sensors described previously, sGC is a heterodimer with the heme center present in the β subunit, and the cyclase active sites present at the interface between the α and β subunits (91). As isolated, ferrous sGC appears to bind NO with a K_D of ~ 4 pM, which is similar to that for NO binding to mammalian Mbs (30, 93). However, the affinity of sGC for CO is 100 million-fold lower, and the observed K_D for CO binding is on the order of 100–300 μM, which is roughly 10,000-fold larger than K_D for CO binding for mammalian Mb (17, 112) (Table 1). More importantly, there is no evidence for the formation of an oxygenated ferrous complex under atmospheric pressure in air or pure O_2. Autooxidation is remarkably slow, and purified sGC does not show any heme optical spectral shift for several weeks at 4°C, even after substantial loss of cyclase activity has occurred. Thus, gas selectivity for sGC appears to be determined almost exclusively at the ligand binding step.

Total exclusion of O_2 is a special property of sGC and is observed for only a few gas sensors, including cyt c′. Four possible mechanisms have been proposed to explain the absence of O_2 binding by ferrous sGC:

1. Lack of a hydrogen-bond donor, such as histidine or tyrosine, on the distal side of the heme to preferentially stabilize bound O_2.
2. A negative electrostatic field adjacent to bound ligands that selectively destabilizes the polar Fe-O_2 complex.
3. Steric restriction of ligand access to the iron atom by distal heme pocket amino acid side chains that directly inhibit bond formation and sterically hinder the bound ligand.
4. Inhibition of in-plane movement of the Fe atom due to an unfavorable Fe-proximal base orientation or other steric restraints that prevent movement of the proximal amino acid toward the heme group.

Preferential Stabilization of Bound O_2 by Hydrogen Bonding and Destabilization by Negative Electrostatic Fields (Mechanisms 1 and 2)

The distal histidine located at the seventh position along the E-helix in Mb has been shown to stabilize bound O_2 over a 100-fold by hydrogen bonding in Mb and Hb (84, 90, 93). Replacing His(E7) with apolar amino acids causes marked, 100-fold decrease in O_2 affinity of mutant Mbs and Hbs (70, 80, 98, 111). In many bacterial and some invertebrate Hbs, a tyrosine at the B10 helical position serves as a strong H-bonding donor to preferentially stabilize bound O_2, and in some of these cases, a glutamine at the E7 position further stabilizes the Fe(II)O_2 complex (16, 30, 38, 45, 76, 89). In these proteins, replacement of TyrB10 by phenylalanine or GlnE7 by leucine markedly increases the O_2-dissociation rate constant indicating loss of these favorable interactions (30, 38, 73, 77).

Marletta and his coworkers have suggested that a lack of H-bonding donors in the distal heme pocket of sGC may account for O_2 exclusion based on their investigations of several other gas-sensing heme proteins that show significant sequence homology with the sGC heme-binding domain (13–15, 87). This hypothesis was proposed based on the structural information from a heme sensor isolated from the anaerobe, *Thermoanaerobacter tengcongensis* (*Tt*), which belongs to the H-NOX family of proteins. The crystal structure revealed a direct H-bond between Tyr140 and bound O_2 and secondary H-bonds from Trp9 and Asn74 to Tyr140 (13–15, 87) (Fig. 1, top). Crystallographic data for the same protein, also called Tt sensor of NO (SONO), obtained by Raman and his colleagues (81) showed different side chain orientations of Trp9 and Asn74, which do not appear to donate H-bonds to Tyr140 (Fig. 1, bottom). However, the bond length between the O atom of Tyr140 and the second O_2 atom of the O_2 is the same in both structures. Bound O_2 is assigned an orientation in the Tt SONO structure almost opposite to that in the *Tt* H-NOX structure (Fig. 1). When Tyr140 is replaced with Leu in *Tt* H-NOX, O_2 affinity decreases more than one order of magnitude, and the double Y140L/W9F mutant shows little or no O_2 binding (13). While involvement of Trp9 and Asn74 in regulating O_2 binding is tenuous, it is clear the Tyr140 stabilizes bound O_2 in this sensor.

Marletta and coworkers have suggested that replacing apolar residues to tyrosines in the heme active sites of NO-binding sensors that normally exclude O_2 can convert them into H-NOX domains that bind O_2 (13). To test this hypothesis, they replaced the apolar isoleucine located in the heme-binding pocket of sGC to tyrosine. They reported that the I145Y mutation in the β subunit heme domain of sGC [β1 (1–385)] allows O_2 binding, but their estimated K_D of $\sim 70{,}000\,\mu M$ demonstrates that O_2 is still excluded from binding to the iron atom under physiological conditions, even when a tyrosine side chain is near the bound ligand (13). Insertion of a tyrosine into the active site of *Legionella pneumophila* H-NOX (L2 H-NOX) gave more definitive results indicating reversible O_2 binding as judged by both kinetics and visible spectra (13).

Based on these mutagenesis results, Marletta and his colleagues concluded that (i) a distal pocket tyrosine is necessary and sufficient for O_2 binding in the H-NOX family and (ii) lack of a distal pocket H-bond donor in sGC eliminates O_2 as a functional ligand, making the sGC H-NOX domain selective for NO. However, we have recently shown that the full-length I145Y mutant of α1/β1-sGC does not show O_2 binding even in buffer saturated with pure O_2 (68) (Fig. 2). In addition, the

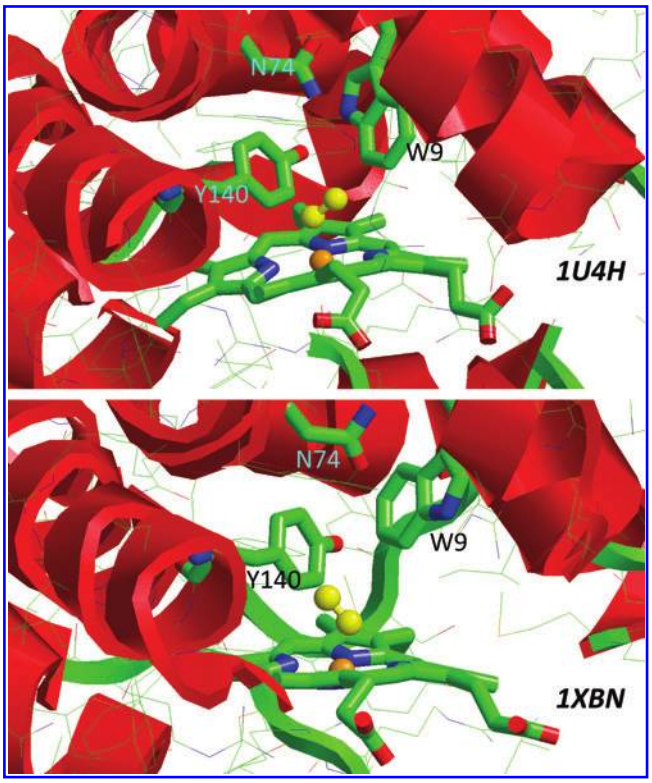

FIG. 1. Structural differences between *Thermoanaerobacter tengcongensis* heme nitric oxide/oxygen-binding domain (*Tt* H-NOX; *top*) and Tt sensor of nitric oxide (SONO; *bottom*) in the heme binding pocket. Same sensor protein was isolated from *Thermoanaerobacter tengcongensis* and structure resolved by two different groups as *Tt* H-NOX (*1U4H*) and SONO (*1XBN*). General folding in the vicinity of the heme site is very similar between these two structures, but the W9 and N74 involved in H-bonding with Y140 in *1U4H* are absent in *1XBN* as the indole and amide nitrogen in W9 and N74 are moved away from the Y140 phenoxyl group. The distance between the phenol oxygen and W9 indole nitrogen is 2.7 and 5.9 Å in *1U4H* and *1XBN*, respectively; the distance between the phenol oxygen and N74 amide nitrogen in *1U4H* is 2.9 Å and to the N74 amide oxygen in *1XBN* is 3.8 Å. The dioxygen (O_2) ligand (*yellow ball/stick*) shows almost opposite orientations relative to the Y140 phenoxyl in these two structures although the distance between the phenol oxygen and the distal O atom of O_2 ligand are similar, 2.5 *versus* 2.7 Å, respectively. (To see this illustration in color the reader is referred to the web version of this article at www.liebertonline.com/ars).

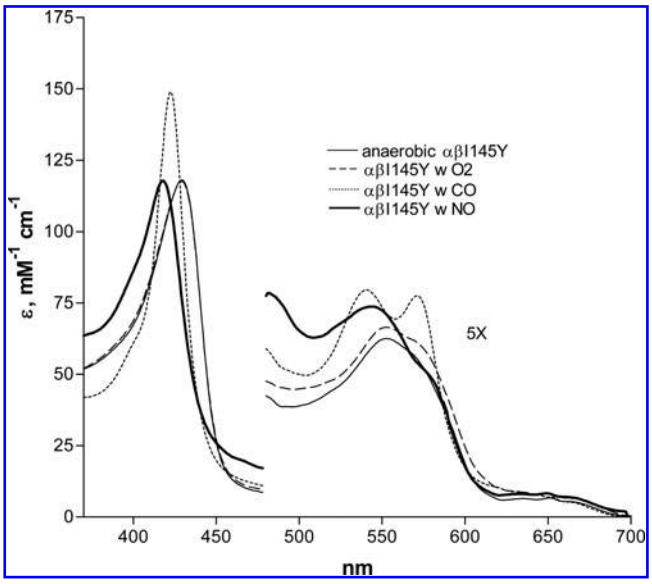

FIG. 2. Electronic spectra of α1/β1-sGC-I145Y. Spectra were recorded in the absence or presence of O_2 (~1 m*M*), carbon monoxide (CO, ~1 m*M*), and nitric oxide (NO, 50 μM).

SONO protein from *Clostridium botulinum* (CB SONO or *CB* H-NOX), which contains a conserved distal pocket Tyr, has an apparent K_D for NO binding of $\sim 10^{-15}$ *M* and still does not bind O_2 (81). Thus, the presence of an active site-tyrosine does not assure O_2 binding.

Similarly, a completely apolar heme site for gas ligands does not necessarily preclude O_2 binding. Replacing the distal histidine in Mb with Val, Leu, Ile, and Phe creates a completely apolar active site and causes a selective ~100-fold increase in the K_D for O_2 binding from ~1 to 50–300 μM (98, 111). However, O_2 binding is easily observed in air or 100% O_2 and facilitates rapid autooxidation (111). Thus, loss of hydrogen bonding by itself cannot account for the complete exclusion of O_2 binding by sGC.

Denninger *et al.* (27) have argued that negative electrostatic fields in the vicinity of the bound ligand could preclude O_2 binding by repulsion of the polar $Fe^{\delta(+)}$-$O_2^{\delta(-)}$ complex. However, sequence homology with the bacterial NO sensors and their structures indicate that there are no electron donors or negative charges in the active sites of these heme proteins, except for the possibility that the nonbonded electrons of the tyrosine Oζ atom in *Tt* H-NOX could be pointing toward the bound ligand and not the hydroxyl H atom. Nevertheless, even when negative fields occur near bound O_2 in V68T Mb (108) and wild-type *Cerebratulus lacteus* miniglobin (88), O_2 binding is still observed.

Direct Steric Inhibition of Ligand Binding (Mechanism 3): Lessons Learned from *Alcaligenes xylosoxidans* Cytochrome c′

The third explanation for O_2 exclusion by sGC is that access to the iron atom is sterically hindered by large distal amino acid side chains. In globins, the direct steric restriction of iron-ligand bond formation appears to uniformly decrease the affinities of all three diatomic ligands (85). This effect is best seen for the Val68 to Ile mutation in Mb, where the Cδ-methyl group lies directly over the iron atom and decreases the affinity of Mb for all three gases by ~5-fold. Similar nonselective effects are seen in Mb and Hb when Leu at the B10 helical position is increased in size to Trp and causes a ~25-fold decrease in all three ligand affinities (12, 86, 93).

Severe steric restriction of ligand binding does occur in cyt c′ from *A. xylosoxidans*, which has biochemical, biophysical, and ligand binding properties that are very similar to those of sGC (59), and for which there is a high resolution crystal structure. There are six similarities between sGC and cytochrome c′ that are relevant to ligand binding (2–5, 37, 49, 67, 71):

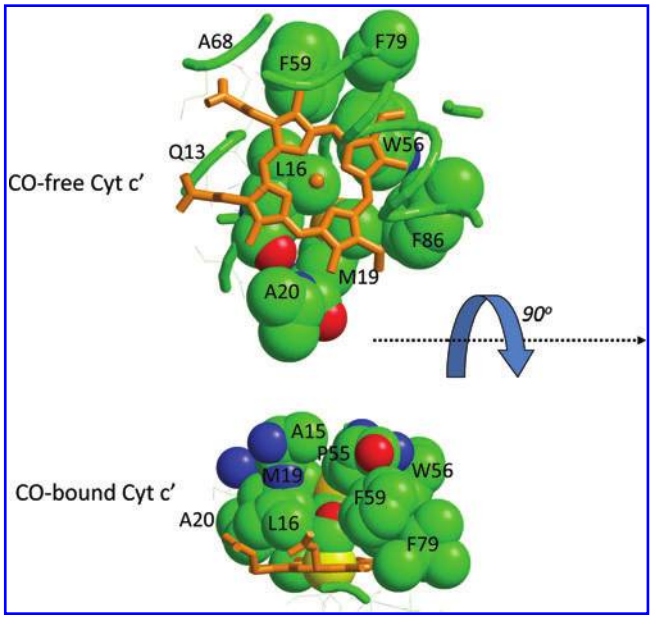

FIG. 3. CO-induced structural changes in the heme pocket of cytochrome c′ (cyt c′). CO-free (*Top*) and CO-bound (*Bottom*) cyt c′ structures reveal the major movement of the sterically hindered L16 and recruitment of P55 into 5 Å of the heme center upon CO binding. Bound CO is slightly tilted due to the proximity of L16. The view of the bottom structure is 90° rotated from the structural view of the *top*. All revealed residues are hydrophobic in nature. (To see this illustration in color the reader is referred to the web version of this article at www.liebertonline.com/ars).

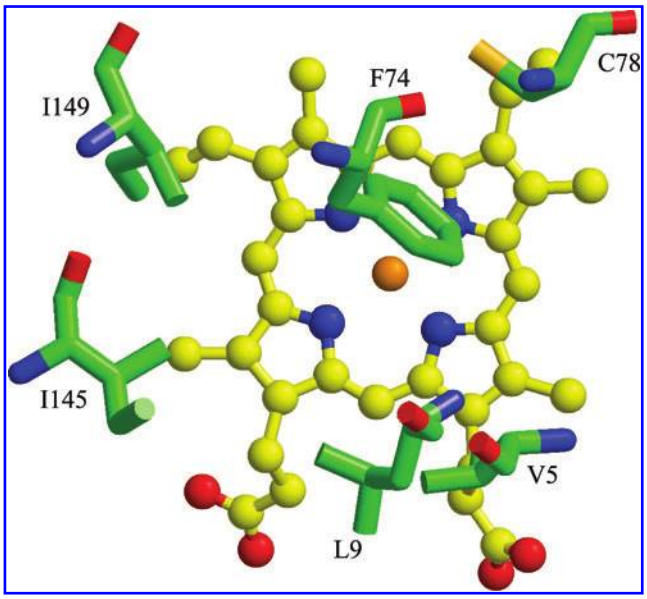

FIG. 4. The main residues predicted to be present in the distal heme pocket of soluble guanylyl cyclase (sGC). Six hydrophobic amino acid residues occupy the distal heme pocket modeled against *Ns* H-NOX crystallographic data to provide an environment where low polarity is expected [adapted from (81)]. (To see this illustration in color the reader is referred to the web version of this article at www.liebertonline.com/ars).

1. Both proteins have very hydrophobic distal heme pockets (Figs. 3 and 4) (59, 81).
2. Both proteins bind CO and NO but not O_2 (Table 1) (49, 113).
3. As isolated, the heme centers of both proteins are 5c high-spin ferrous iron (3, 112).
4. The K_Ds for CO binding are much greater than those for other reduced, high-spin hemeproteins with a proximal histidine ligand, and the association rate constants for CO binding are very small (50, 112, 114).
5. The ferric form of each hemeprotein shows poor cyanide and azide binding in comparison with Mb or model hemes (50, 75, 115).
6. NO binding first forms a six-coordinate NO complex (6c-NO) complex and then transforms to a five-coordinate NO complex (5c-NO complex). The conversion from 6c-NO complex to 5c-NO complex is dependent on [NO] for both proteins, indicating a two-step scheme, both of which involve NO binding (2, 131).

Steric constraints in the distal pocket appear to be the key factor repressing O_2 binding to cyt c′, and extensive ligand binding (49) and resonance Raman (rR) and Fourier transformed infrared spectroscopy studies (3, 4, 37) and quantum mechanics/molecular mechanics computations (67) support this hypothesis. Comparison of the crystallographic data of the CO-free and CO-bound forms of cyt c′ from *A. xylosoxidans* (AXCP) suggest that the side chain of Leu16 blocks access to the iron atom and must be pushed away from the center of the heme ring to accommodate bound CO (6). This movement also causes extensive rearrangements of other distal residues, including Pro55 (Fig. 3). Antonyuk *et al.* (6) have shown that this steric hindrance decreases CO affinity 4 to 5 orders of magnitude compared to that for heme models or Mb, and the value of the K_D for CO binding to cyt c′ is very similar to that for sGC (67) (Table 1).

These workers have recently shown that L16A and L16G mutations in cyt c′ decrease K_D(NO) and K_D(CO) to remarkably small values, $\sim 70\times10^{-15}$ and $\sim 3\times10^{-12}$ *M*, respectively. Most remarkably, these cyt c′ variants bind O_2 with high affinity, $K_D(O_2) \approx 50$ n*M* (Table 1) (6, 36). Such high ligand affinities indicate that the intrinsic reactivity of the heme iron in cyt c′ is very high as previously suggested by theoretical calculations (6, 67). Thus, the severe restriction of O_2 binding in wt cyt c′ is due exclusively to the *iso*-butyl side chain of Leu16, which also reduces the stability of 6c-CO and -NO complexes.

In contrast to CO binding, the reaction of NO with reduced cyt c′ is complex and involves formation of an initial unstable hexacoordinate complex, which shows a very poor affinity for NO (*i.e.*, $K_D \approx 0.1$–1 μM, Table 1) (2, 36, 37). Then, the proximal imidazole bond breaks, a second NO binds to the iron from the proximal pocket, displacing the original ligand on the distal side to form a stable 5c-NO complex. In this equilibrium 5c complex, the bound NO is on the proximal side of the heme. The preference for NO binding on the proximal side appears to be a consequence of the highly congested distal pocket, due primarily to Leu16 and stabilization of bound NO by Arg124 on the proximal side of the porphyrin ring (36, 59). The binding of a second NO in the proximal pocket to create a transient NO-heme-NO species provides the basis for the [NO] dependence of conversion from 6c- to 5c-NO complex (2, 67).

Proximal Coordination Geometry and Inhibition of Ligand Binding (Mechanism 4)

The fourth proposal for O_2 exclusion is that steric constraints on the proximal side of the heme inhibit in-plane movement of the iron atom, weaken the pentacoordinate Fe-proximal His bond, and greatly inhibit formation of hexacoordinate complexes with all three ligands. However, NO is capable of forming a strong pentacoordinate complex and breaking the sterically-restricted Fe-proximal His bond, whereas CO and O_2 cannot. Consequently, a high affinity 5c NO-heme complex can be formed by displacing the proximal histidine. This idea was first proposed by Traylor, Sharma, and colleagues in the 1980–1990s (106, 107, 119), and is supported by the multi-step NO binding scheme proposed for cyt c′ and by multiple electron paramagnetic resonance (EPR) and resonance Raman (rR) studies, which show that at equilibrium, the sGC-NO complex is pentacoordinate (25, 28, 64), as represented in Figure 8.

The stretching frequency of the Fe-His bond in the ligand-free reduced sGC is 204 cm^{-1}, which is at the low end of all known measurements, where ν(Fe-His) ranges from 200 to 300 cm^{-1} (129). In many other proteins, the presence of an H-bond acceptor adjacent to the proximal histidine Nδ-H atoms usually increases the Fe-imidazole bond strength by $\sim$20 cm^{-1} due to enhanced basicity of the coordinating Nε atom (89). In sGC, weak π-donation by the histidine Nε atom causes weak Fe dπ donation to O_2 π^*. There is weak linear correlation between ν(Fe-His) and ν(Fe-O) for model heme compounds (30), but rR data for the Fe-His stretching of *VC* H-NOX and *Tt* H-NOX are opposite to the observed O_2 binding capability of these two heme sensors (48). Moreover, a low value of ν(Fe-His) does not necessarily predict O_2 exclusion. Many heme-proteins have a weak Fe-His bond but can easily bind O_2. For example, some deoxygenated model Fe(II)PPIX complexes have ν(Fe-His) = 201–205 cm^{-1} but still show moderate O_2 affinities (23, 129). FixL($\nu_{Fe\text{-}N\varepsilon}$ = 208 cm^{-1}) (118), T-state α-chain Hb ($\nu_{Fe\text{-}N\varepsilon}$ = 207 cm^{-1}) (79), ovine prostaglandin H synthase, or oPGHS-1, ($\nu_{Fe\text{-}N\varepsilon}$ = 206 and 225 cm^{-1}) (62, 105) also have Fe-His bond strengths similar to that of sGC but bind O_2 under physiological conditions. Ferrous o-PGHS-1 reacts readily with O_2 and autooxidizes rapidly to form ferric prostaglandin H synthase type 1 (PGHS-1) (Tsai *et al.*, unpublished results). Tomita and his colleagues have concluded that there is no correlation between Fe-His bond strength as measured by ν(Fe-His) and O_2 binding parameters (118).

Even if the Fe-His bond is strong in the pentacoordinate reduced state, there may be large steric restraints to the in-plane movement of the iron that is required for O_2 and CO binding. As result, both the Fe-His and Fe-ligand bonds can be weakened markedly in hexacoordinate low-spin complexes, and there is strong evidence that this occurs in sGC (118). The sGC-CO complex exhibits the lowest Fe-CO stretching (472 cm^{-1}) that has been observed for heme proteins containing a neutral proximal histidine (25), and the weak Fe-CO bond correlates with the very large CO dissociation rate constant (k_{off}) observed for this protein (Table 1) (13, 68, 112). The remarkably large k_{off}(CO) value cannot be the result of an apolar pocket because hydrogen bonding to bound CO is weak and can only stabilize the bound ligand by a factor of 2–5 based on mutagenesis studies with Mb (60, 90). In contrast, the proximal constraints associated with the R to T transition in human Hb cause k_{off}(CO) to increase 20-fold from 0.01 to 0.2 s^{-1} (124), and even larger effects have been observed for model hemes with proximal constraints (119). Thus, proximal constraints do play a very significant effect in regulating ligand binding affinity.

Lessons from *Nostoc* H-NOX, a Structurally Homologous Sensor to sGC

The recent crystal structure of *Ns* H-NOX has provided very useful insights into ligand selectivity by gas sensors (63). *Ns* H-NOX, (also called NP-SONO) has the highest sequence identity (31%) and structural homology with the sGC heme domain compared to the other SONOs from *C. botulinum* and *T. tengcongensis* (81). The proposed model for the heme pocket for sGC is similar to that reported for *Ns* H-NOX. Six hydrophobic amino acid residues line the distal heme pocket and are highly conserved even in their side chain orientations (V5/V5, I9/L9, F70/F70, W74/F74, M143/I145, and L147/I149, respectively, for *Ns* H-NOX/sGC), and the only polar amino acid (T77/C78) also appears to adopt the same side chain orientation relative to the heme porphyrin by molecular modeling (Fig. 4).

However, a recent spectroscopic and kinetic study revealed interesting differences in gas binding to *Ns* H-NOX *versus* sGC (122). *Ns* H-NOX sequentially forms two different but relatively stable 6c-NO complex intermediates with Soret absorption peaks at 418 and 414 nm, respectively, after mixing the unliganded, reduced 5c complex with NO. Formation of the second 6c-NO complex also shows dependence on [NO], indicating a complex multi-step mechanism. Only partial conversion to 5c-NO complex occurs even with excess NO (122). The restricted formation of the 5c-NO complex in *Ns* H-NOX, and the substantial conformational change upon heme oxidation implies that *Ns* H-NOX may be a redox sensor rather than an NO-sensing protein. In addition, *Ns* H-NOX binds O_2 very weakly and autooxidizes slowly (122), whereas sGC is totally inert to O_2.

The major structural difference between the heme pockets of *Ns* H-NOX and sGC appears to be the replacement of a Trp74 in H-NOX by a Phe74 near the heme iron in sGC (63) (Fig. 5A). In the CO- and NO-bound *Ns* H-NOX structures, the indole ring of Trp74 is in van der Waal's contact with the gaseous ligand, and the indole nitrogen may serve as a H-bond donor to the nitrogen atom of bound NO (the oxygen atom of NO does not appear to be properly aligned for H-bonding even though it is closer in distance) (Fig. 5B, C). The bulky Trp74 side chain appears to cause an $\sim$15° tilt from a perfect linear Fe-CO geometry. The same steric effect likely causes a Fe-N-O angle of $\sim$150° rather than a 120° bent conformation predicted by the rule of Feltham and Enemark. The equivalent residue for sGC is Phe74, which is less bulky and has no H-bonding donor capability.

The presence of a Trp74 H-bond donor may provide a stabilization mechanism for the observed 6c-NO complexes in *Ns* H-NOX, and the H-bonding would favor the bent form of NO and a less negative trans effect. Such stabilization of the 6c-NO-sGC complex by Trp74 may account for the lower NO-dependent activation observed for the α-βF74W sGC mutant (63). Careful kinetic measurements for NO and CO binding to wild-type *Ns* H-NOX, its W74F mutant, and to the $\alpha\beta$F74W sGC should provide a clearer picture of the role of residue74 in ligand selectivity.

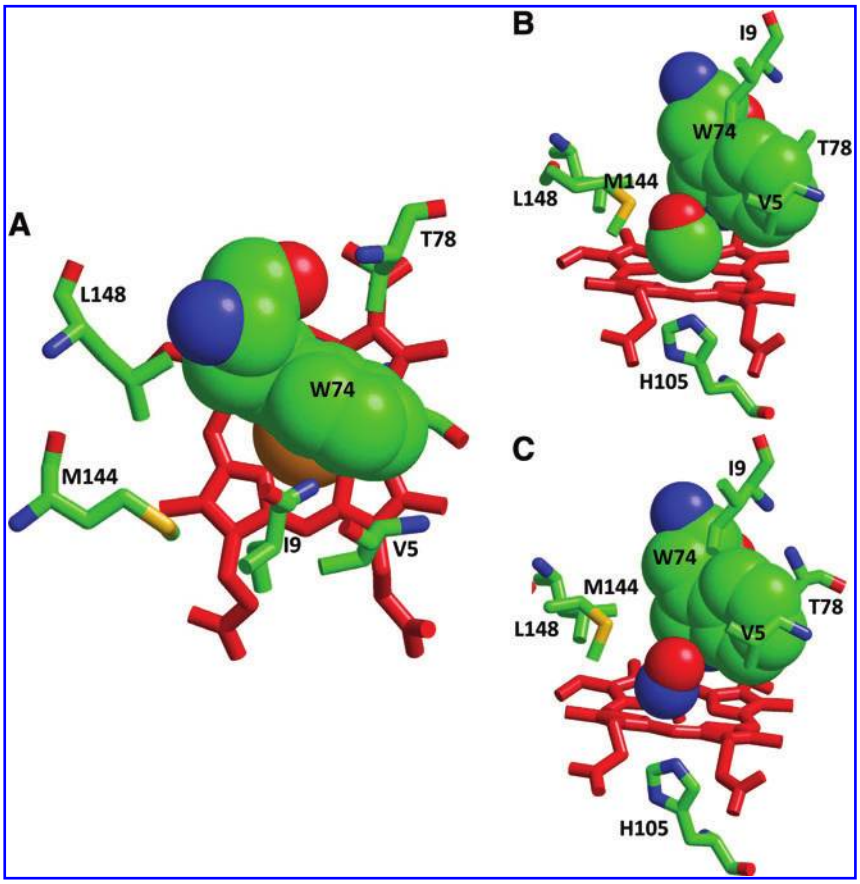

FIG. 5. Key residues in the heme distal pocket of ligand-free *Ns* H-NOX (A), and its CO-bound (B), and NO-bound (C) forms. *Top* view of the ligand-free sensor and side views of the ligand-bound sensor are provided with the key Trp74 and the CO and NO ligands shown in space-filling model to show the influence of Trp74 in steric constraint on ligand binding geometry. Protein Data Bank (PDB) codes for the free, NO- and CO-bound *Ns* H-NOX are 2O09, 2O0C and 2O0G, respectively. (To see this illustration in color the reader is referred to the web version of this article at www.liebertonline.com/ars).

The Sliding Scale Rule for NO, CO, and O_2 Binding Affinity to 5c Heme Proteins with a Neutral Proximal Imidazole Base

To understand the unusually high affinity for NO but complete exclusion of O_2 by sGC, we quantitatively examined the relationship between ligand binding parameters and the chemical nature of the gas ligand for >75 different single and multiple variants of globins, heme proteins, and model heme compounds (120). Plots of the logarithm of K_D *versus* ligand species for the series NO, CO, and O_2 yield sets of parallel lines for heme proteins containing a neutral proximal histidine side chain and samples of these data are shown in Figure 6. The absolute K_D values are spread over a vertical range of 8–9 orders of magnitude. The highest affinities and lowest K_D values are observed for L16A cyt c′, in which distal steric hindrance was alleviated by an alanine replacement (36) and H61L leghemoglobin (Lba) mutant, which has a completely apolar and unhindered distal pocket (41). The lowest affinities and highest K_D values were observed for wild-type cyt c′, wild-type sGC, and sGC with site-specific replacement of isoleucine by a tyrosine on residue 145 (I145Y sGC) (Fig. 6). The K_D values for chelated model heme, unhindered Mb mutant (H64V), and *Ns* H-NOX lie in between the two limits. The slopes of the lines for log(K_D) *versus* ligand type, from NO to CO to O_2, show that, in general, there is a ~3- to 4-order separation between the K_D values of NO and CO and between those for CO and O_2 (Fig. 6). This parallel relationship of log K_D for the three gases occurs over a dynamic range of 8–9 orders of magnitude for the individual equilibrium dissociation constants. This linear relationship describes a sliding scale rule for ligand discrimination that applies to all heme proteins containing a neutral proximal imidazole ligand and an apolar distal pocket (121).

The most remarkable result in Figure 6 is the effect of the L16A mutation on ligand binding to cyt c′. Relief of distal steric hindrance by replacement of Leu16 with either alanine or glycine in cyt c′ moved the K_D values of all three gas ligands from the upper (weakest affinity) to the lower (highest affinity) limits of the log(K_D) *versus* ligand plot. This result demonstrates dramatically the critical role of steric hindrance by the Leu16 side chain in regulating ligand access to and dissociation from the heme iron in this bacterial heme sensor. Once steric restriction is removed in cyt c′, the heme iron shows an affinity for ligands that is as high as that of the unhindered leghemoglobin (H61L lb). The cause of the ultra-high affinity of the cyt c′ mutant is the staggered geometry of the proximal histidine ring with respect to the pyrrole N atoms (6, 36, 43), which is compared to the eclipsed geometry found in Mb in Figure 7b. Soybean Lb shows a similar staggered proximal geometry (41, 56, 57), and a variety of mutagenesis and kinetic studies have shown that this conformation accounts for the high reactivity of Lb with all ligands compared to Mb (41, 56, 57). In wt cyt c′, the iron atom is still highly reactive, but the binding of all ligands is dramatically inhibited by the sterically restricted distal active site, in which the *iso*-butyl side chain of Leu16 is held rigidly over the axial position of the heme iron atom (Fig. 3).

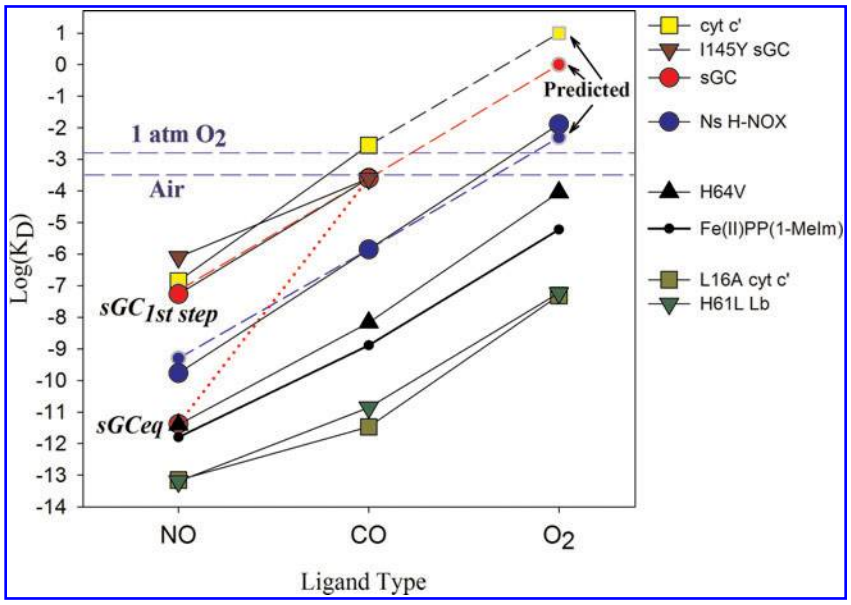

FIG. 6. Sliding scale rule principle revealed by graphical analyses of K_D, versus ligand types. K_D values for cyt c′ (*yellow squares*), I145Y sGC (*maroon reversed triangles*), sGC (*red circles*), *Ns* H-NOX (*blue circles*), H64V Mb (*black triangles*), Fe(II)PP(1-MeIm) model heme (*black circles*), L16A cyt c′ (*dark yellow squares*), and H61L Lb (*green reversed triangle*) are plotted against NO, CO, and O_2 ligands on a logarithm scale to show the ~8-order of magnitude dynamic range of the binding parameter values. Other than the unusually low value of K_D(NO) for sGC (*red circles* and *red lines*), the general relationship between the different heme proteins are parallel lines for all three ligands. The estimated K_D(NO), $K_D(O_2)$ values, for sGC, cyt c′, *Ns* H-NOX based on the sliding scale rule are also highlighted (*dashed lines*). O_2 concentrations of air-saturated buffer and O_2-saturated buffer are indicted by *horizontal blue dashes*. (To see this illustration in color the reader is referred to the web version of this article at www.liebertonline.com/ars).

Deviations from the Sliding Scale Rule: sGC and Ultra-High O_2 Affinity Globins

The major outlier from the sliding scale rule shown in Figure 6 is the sGC. Despite a K_D(CO) similar to that for cyt c′ and I145Y sGC, the reported overall equilibrium dissociation constant for NO binding to sGC is ~5 orders lower than that predicted by a line parallel to the data for all the other heme proteins. This deviation from the sliding scale rule led us to reassess the literature value for the NO binding equilibrium constant. The reported value for K_D(NO) value for sGC was calculated as the ratio between the k_{off} for the final equilibrium 5c-NO complex and the k_{on} for the initial 6c-NO complex formed on mixing unliganded ferrous sGC with NO anaerobically (52, 131). Thus, the K_D(NO) value does not represent the equilibrium dissociation constant for the initial 6c-NO complex (Fig. 6, $sGC_{1st\ step}$) but instead is an estimate of the K_D value for the overall reaction to form the final 5c complex (see Fig. 6, sGC_{eq}).

Determination of the K_D for the initial 6c-NO sGC complex, which should be predictable by the sliding scale rule analysis in Figure 6, requires accurate measurement of the NO association (k_{on}) and dissociation (k_{off}) rate constants for the formation of this transient intermediate. Using rapid multimixing methods, we determined k_{on} and k_{off} to be 4.8×10^8 $M^{-1}s^{-1}$ and $27\,s^{-1}$ at 24°C for the initial 6c NO-heme-His complex of full length sGC (121). Thus, the K_D(NO) for the initial 6c-NO complex is 5.4×10^{-8} *M*, which is similar to the K_D values for the initial and more kinetically stable 6c NO complexes of cyt c′ and I145Y mutant of sGC (37, 68, 122) and the value predicted by the sliding scale rule with the K_D for CO binding (Fig. 6, red circle).

This correlation between the predicted and observed K_D values for the 6c-NO complex of sGC supports the use of the sliding scale to estimate the K_D value for O_2 binding to sGC. As shown in Figure 6 (red dashed line and red circle with grey edge), the predicted K_D for O_2 binding to sGC is ~1 *M*, way above the O_2 concentration of air- or even O_2-saturated buffer. Similar high $K_D(O_2)$ values are predicted for I145Y sGC and cyt c′ (~10 *M*, Fig. 6), and thus the sliding scale rule and the measured values of K_D(NO) and K_D(CO) for 6c complexes empirically predict the exclusion of O_2 binding to these proteins under aerobic conditions.

As a test of the validity of the sliding scale rule, we looked for O_2 binding to *Ns* H-NOX at high O_2 pressures. *Ns* H-NOX was chosen because of its lower K_D for CO binding (Fig. 6) and because it does slowly autooxidize at a rate of $0.05\,h^{-1}$, indicating some reactivity with O_2 in air (122). Linear extrapolation of the line connecting the log K_D values for NO and CO binding to *Ns* H-NOX predicts a K_D for O_2 binding of ~15 m*M* (blue circle with grey edge in Fig. 6). We then examined O_2 binding to *Ns* H-NOX experimentally using a high-pressure cell and obtained an isotherm with a $K_D \approx 13$ m*M* (Fig. 6, blue circle) (121), which matched almost exactly the prediction from the sliding scale rule. Thus, the sliding scale rule applies to the 6c complexes of all three of the NO sensors and predicts empirically that none of them can bind O_2 under physiological conditions.

There are other dramatic deviations from the sliding scale rule due to selective lowering of the $K_D(O_2)$ values for globins

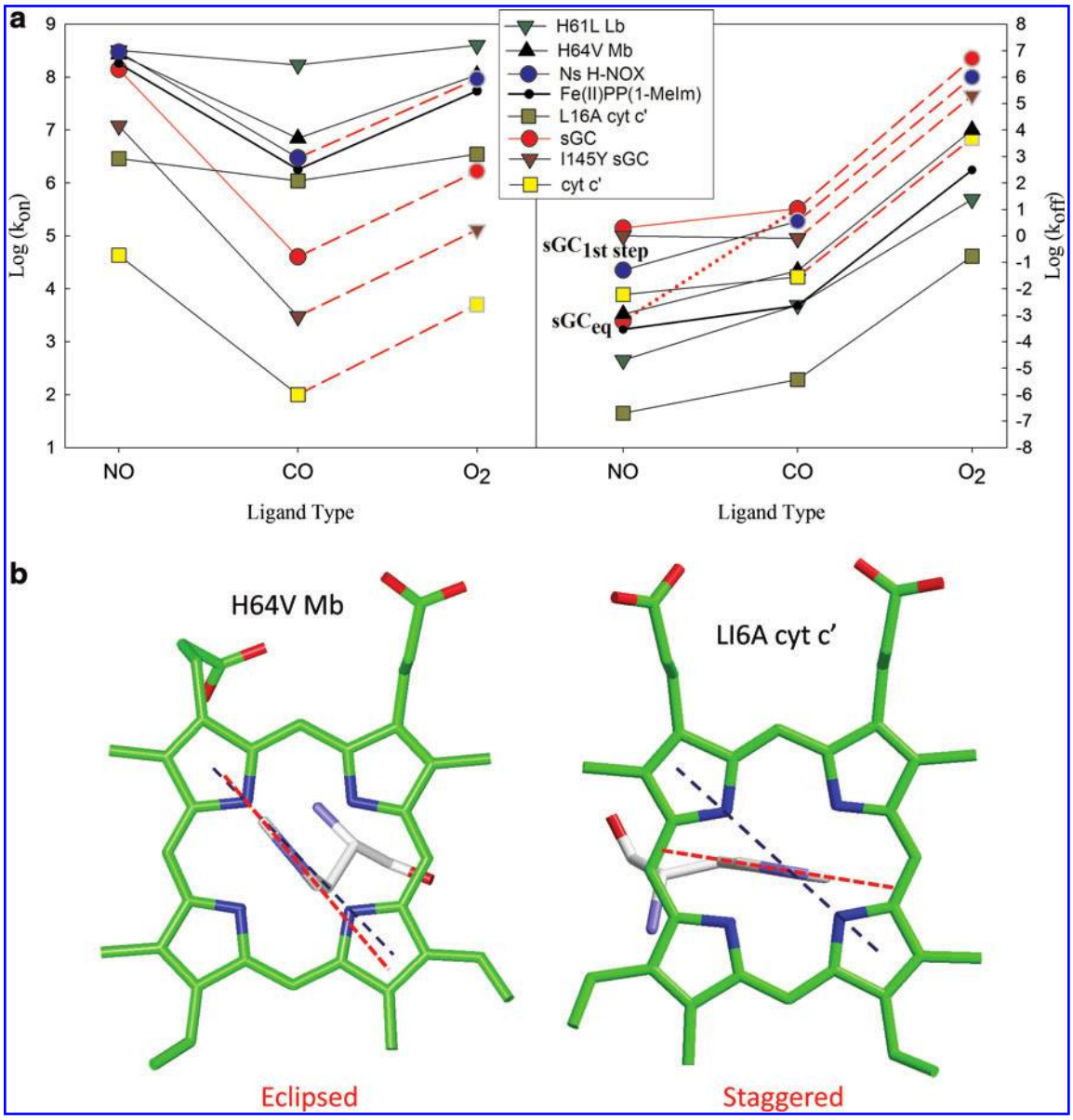

FIG. 7. Sliding scale rule graphical analyses of k_{on} and k_{off} against ligand types and the ring orientation of the proximal His ligand. k_{on} (**a**, *left*) and k_{off} (**a**, *right*) values for the same set of hemeproteins shown in Figure 6 are plotted against NO, CO, and O_2 ligands in logarithm scale to show the V-shaped and reversed L-shaped sliding scale relationship for the k_{on} and k_{off} values. The estimated k_{off}(NO) and k_{off}(O_2), for cyt c′, I145Y sGC, sGC, and *Ns* H-NOX based on the sliding scale rule were also highlighted (*red dashed lines*). The ring orientations of the proximal His ligands, His93 and His 120, respectively, relative to the heme porphyrin macrocycle in H64V Mb and L16A cyt c′ are shown in **b**. This top down view of heme and proximal histidine ligand reveals the eclipsed and staggered conformations between the imidazole ring (*red dashes*) relative to the line connecting the nearest pair of two pyrrole nitrogen atoms (*blue dashes*). PDB codes are 2mgj (H64V Mb) and 2yl0 (L16A cyt c′). (To see this illustration in color the reader is referred to the web version of this article at www.liebertonline.com/ars).

as result of selective stabilization of the polar Fe-O_2 complex (121). This selective discrimination in favor of O_2 binding has been the focus of extensive study over the past 30 years and is due to electrostatic stabilization of bound O_2 by hydrogen-bonding with distal amino acids, most noticeably distal E7 His and Gln and B10 Tyr side chains in the globin family of heme proteins (84, 93). This selective stabilization is absent in mutants, where His(E7), Gln(E7), and Tyr(B10) are replaced with apolar amino acids, (*i.e.*, the H64V Mb mutant in Fig. 6) (121).

Sliding Scale Rules for Ligand Association (k_{on}) and Dissociation Rate Constants (k_{off})

We carried out similar correlation graphical analyses of the k_{off} and k_{on}, rate constants for NO, CO, and O_2 binding to the same large library of heme proteins. As shown in Figure 7a (left panel), a set of parallel V-shaped lines are observed for plots of log(k_{on}) *versus* NO, CO, and O_2, with absolute values spanning 5–6 orders of magnitude and k_{on}(CO) always showing the lowest value (120). There are two reasons why

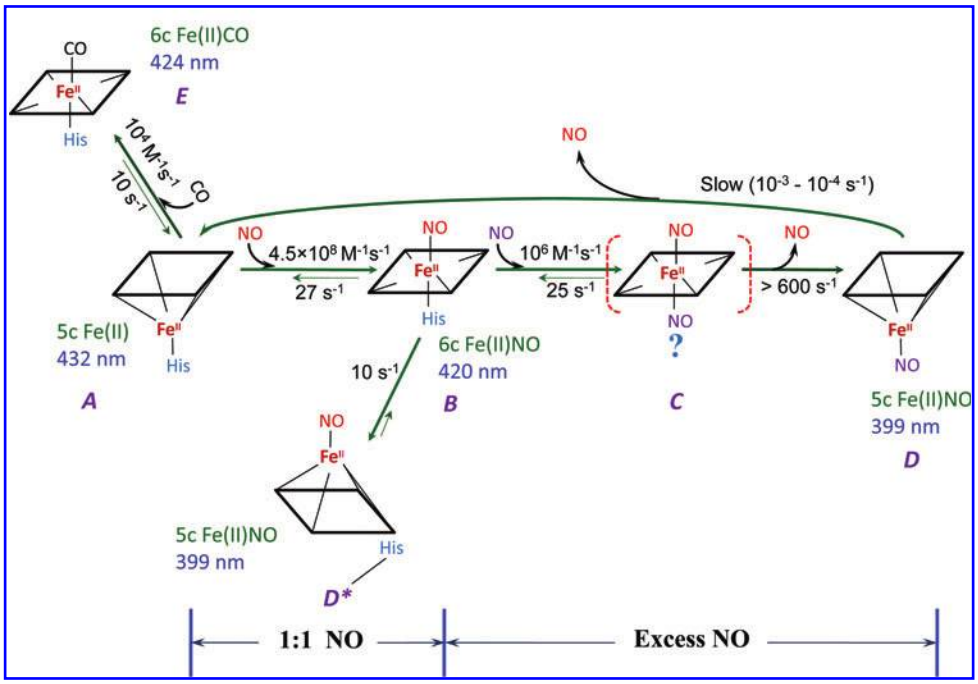

FIG. 8. Single- and multiple-binding interactions between sGC and CO and NO, respectively. Resting sGC, present as a 5c high-spin species (A), exhibits 1-step reversible binding with CO to form a 6c complex (*E*). For NO binding to sGC, in addition to a similar 6c complex (B), two 5c-NO complexes are observed (D* and D) at NO stoichiometry ≤1 and >1, respectively. The irreversible steps of NO binding (B→D* and C→D) resulted in an overall enhanced binding affinity. Bis-NO complex (C) formation is supported by the fact of [NO]-dependent 2nd step (B→C) and recent ligand binding study using $^{15}NO/^{14}NO$ and sequential freeze-quench electron paramagnetic resonance (EPR) measurements (132). The rate constants of each chemical step are from our kinetic measurements at 24°C. (To see this illustration in color the reader is referred to the web version of this article at www.liebertonline.com/ars).

CO shows the lowest k_{on} relative to NO and O_2. First, the in-plane movement of the heme iron is required to vacate the electron in the d_{z2} orbital to accommodate two electrons from the nonbonding orbitals of CO; and second, the spin-forbidden nature of iron-carbonyl bond formation markedly increases the activation barrier (33, 116). In contrast, bond formation can occur without a spin-state change of the iron when NO and O_2 are the ligands, because both contain unpaired electrons in the HOMO (46). The bimolecular association rate constant for NO binding is limited almost exclusively by the speed of ligand movement to the iron atom, whereas CO binding can be limited by rates of iron movement into the heme plane and bond formation, which can be slow relative to diffusion of the ligand into the protein. O_2 binding can be limited by both processes, but in many cases, $k_{on}(O_2)$ is similar to $k_{on}(NO)$.

Soybean H61L Lb sets the upper limit of the V k_{on} relationship and wild-type cyt c′ sets the lower limit, representing totally free and completely sterically-restricted access to the iron atom, respectively. Steric constraints from the protein structure clearly plays a dominant role in inhibiting ligand binding to cyt c′, regardless of which ligand is examined. Replacement of Leu16 with Ala causes a 2–5 order of magnitude increase in k_{on} for the binding of all three gas ligands to cyt c′ (Fig. 7a, left panel). Interestingly, both cyt c′ and Lb mutants show similar shallow k_{on} dependences on ligand type, with $k_{on}(CO)$ being large and much closer to $k_{on}(NO)$ and $k_{on}(O_2)$. This behavior is indicative of a highly reactive iron atom, high rates of bond formation, and diffusion limitation of ligand association. Even though their K_D values are almost identical, the k_{on} values for L16A cyt c′ are uniformly ~2 orders of magnitude smaller than those for ligand binding to H61LlLb. Thus, movement into the active site of L16A cyt c′ is still restricted by the densely packed amino acid side chains surrounding the active site (Fig. 3).

Graphical analyses of k_{off} values *versus* ligand type are also shown in Figure 7a (right panel). The parameter values can be represented as a set of parallel reversed L patterns. The general trend is that $k_{off}(O_2)$ is much larger than either $k_{off}(NO)$ or $k_{off}(CO)$, and in most cases, $k_{off}(NO)$ is 10- to 100-fold lower than $k_{off}(CO)$. The k_{off} values indicate the stability of the ligand-bound complex, and the lack of backbonding capability of O_2 relative to NO and CO is the basis for its faster dissociation from the heme iron. CO can use both π^* orbitals for backbonding, which greatly strengthens the Fe-CO bond. NO only has one π^* orbital and one extra electron available compared to CO, and its backbonding strength is not much weaker than CO (24). Relief of one antibonding interaction by losing one backbonding interaction in the bonding plane is offset by a stronger backbonding in the perpendicular plane (y-z plane) with a lower energy π^*. Thus, even though the bent form of Fe(II)-NO seems to be favored over the linear form according to the Feltham and Enemark rule (31), the energy difference between these two forms is not large and is subject to fine tuning by the protein environment. This extra flexibility and the radical nature of NO probably enhance the stability of the NO complex, matching that of the CO complex. The decreased value of $k_{off}(NO)$ compared to $k_{off}(CO)$ is due

primarily to high rate of NO-Fe bond reformation within the protein after thermal dissociation compared to the rate of ligand escape from the protein (82, 83).

The k_{off} values for the 6c-sGC complexes define the upper limits in these plots, and remarkably the k_{off} values for L16A cyt c′ define the lower limits (Fig. 7a, right). The $k_{off}(O_2)$ for sGC is expected to be large based on its predicted K_D, $\sim 1M$ (Fig. 6). We estimate that the $k_{off}(O_2)$ for sGC is 10^7–10^8 s^{-1} based on the product of k_{on} and the projected K_D value (Fig. 7a, right). Again, the most remarkable result is the dramatic ~ 5 order of magnitude decrease in k_{off} for ligand dissociation from cyt c′ due to the L16A mutation. It is clear that distal steric hindrance greatly destabilizes bound ligands in the w.t. cyt c′ complex causing dramatic increases in the rates of thermal breakage of all the iron-ligand bonds. When Leu16 is removed, even O_2 binds with a high affinity (K_D of 49 nM, Table 1) and a low dissociation rate constant (36). The reversed L sliding scale rule applies to this cyt c′ mutant, which shows lines parallel to the heme, Lb, and Mb model systems. Assuming the same parallel relationship, the value of $k_{off}(O_2)$ for wild-type cyt c′ was estimated to be $\sim 5000\ s^{-1}$, which is similar to what would be obtained from the predicted values of $k_{on}(O_2)$ and $K_D(O_2)$ from the sliding scale rule analyses of the data in Figures 6 and 7a, left panel.

The Basis of Ligand Discrimination in NO Sensors

The graphical sliding scale analyses demonstrate that ligand discrimination is built into the chemistry of 5c heme complexes with a neutral imidazole side chain. There are intrinsically ~ 3 to 4 orders of magnitude separation between the affinities of the NO/CO and CO/O_2 pairs. Except for preferential electrostatic stabilization of bound O_2, adding protein around the heme either uniformly reduces or uniformly enhances the affinities of the protein for all three gaseous ligands by changing steric hindrance on the distal side or altering the Fe-imidazole geometry on the proximal side of the porphyrin ring. In the case of sGC, adding a polar distal tyrosine by the I145Y mutation had little effect on the relative or absolute affinities for CO and O_2, suggesting that electrostatic interactions play a minor or no role in regulating ligand binding in this sensor (Fig. 6).

The large K_D values for the binding of all three gaseous ligands to wild-type sGC and cyt c′ appear to be due to severe proximal constraints on iron reactivity and marked steric hindrance of bound ligands on the distal side of the heme plane, respectively. The observed k_{on} value for the initial step of NO binding to w.t. sGC is in the range of 100 to 400 $\mu M^{-1}s^{-1}$, indicating little or no resistance to movement into the distal pocket or access to the iron atom from the distal side of the heme (Table 1) (123, 131). Similar large values for k_{on}(NO) are observed for the unhindered model heme, H64V Mb, and H61L Lb (Table 1, Fig. 7a, left panel). The I145Y sGC mutation does decrease k_{on} for NO binding to 15 $\mu M^{-1}s^{-1}$, a value similar to that for NO binding to wt Mb (Table 1), presumably because the large Tyr side chain does begin to restrict movement to the iron atom. In contrast, the observed bimolecular rate constant for NO binding to cyt c′ is only 0.04 $\mu M^{-1}s^{-1}$, which is a 10,000-fold smaller than that for NO binding to sGC. Replacement of Leu16 with Ala in cyt c′ causes an increase in k_{on}(NO) to 3.0 $\mu M^{-1}s^{-1}$. Thus, it is clear that cyt c′ excludes O_2 binding by severe distal steric hindrance.

The structural mechanism for exclusion of O_2 and the poor affinity of CO for sGC are not as well established, but all the observed data suggest that proximal constraints dramatically lower the reactivity of the heme iron, as originally proposed by Traylor and Sharma over 30 years ago (119). Indeed, Shiro and coworkers (65) have recently emphasized that the heme proximal strain, which limits iron movement toward the porphyrin plane, is the crucial effect that leads to the ultra-weak affinity of sGC for O_2. The exceptionally positive midpoint potentials (E_M) of +187 mV and +234 mV for sGC from humans and *Manduca sexta* support the idea of restriction of in-plane movement of the iron atom during oxidation, which in turn favors the reduced pentacoordinate, out of plane geometry (34, 65). Thus, cyt c′ and sGC have evolved structurally distinct mechanisms to achieve O_2 exclusion, that is, severe distal steric hindrance *versus* proximal strain, respectively.

A Multi-Step Mechanism Evolved to Achieve High NO Affinity When O_2 Binding Is Excluded

Most heme protein sensors need to respond to low nanomolar levels of NO under aerobic conditions. O_2 exclusion is required to prevent both autooxidation and more importantly NO dioxygenation to nitrate, which would rapidly remove the signaling molecule without eliciting the desired physiological effect (*i.e.*, smooth muscle relaxation in the case of sGC). As described in the last section, cyt c′ achieves O_2 exclusion by physically inhibiting ligand binding at the distal axial position, whereas sGC appears to limit the binding of O_2 by inhibiting in-plane movement of the iron atom. Both mechanisms severely inhibit formation of 6c-ligand complexes and markedly increase the K_D values for all ligands as shown in Figure 6. In order to increase the sensitivity to low levels of NO, these proteins evolved mechanisms to form high-affinity 5c-NO complexes with the ligand bound on the proximal side of the heme group.

Hough *et al.* (43) have provided a detailed multi-step mechanism for high affinity NO binding to cyt c′, based on ultra-fast kinetic measurements by Negriere's group (55) and their own mutagenesis and crystallographic studies. The first step involves bimolecular NO binding to form an initial 6c NO-heme-His complex, which is followed by a second catalytic, bimolecular NO binding process to form a highly transient and an unstable NO-heme-NO complex with the proximal His displaced. A final rapid, first order dissociation of the distal NO generates the final equilibrium 5c heme-NO complex (43). The second and third steps are driven by steric hindrance in the distal pocket of cyt c′, which forces the NO to the proximal side of the protein. CO is greatly inhibited and O_2 is effectively excluded because 5c complexes with these ligands are extremely weak.

Animal sGCs evolved a similar multi-step binding mechanism to achieve high affinity NO binding, even though O_2 exclusion appears to be achieved by proximal constraints of in-plane iron movement and not distal steric hindrance (Fig. 8). Again, the initial reaction of NO with ferrous sGC (with a 432 nm Soret peak, species A in Fig. 8) generates a weak 6c Fe(II)NO complex (420 nm Soret, species B in Fig. 8). A distal 5c Fe(II)NO complex (399 nm Soret) forms at low NO:heme stoichiometries (≤ 1) (species D* in Fig. 8), presumably due to the strong proximal constraints that greatly weaken the Fe-

Table 2. Qualitative Summary of the Mechanisms for O_2 Discrimination and/or High Affinity NO Binding by sGC, Cytochrome c′, *NS* H-NOX, Mb, and Heme Models

Protein \ *Factor*	*Physiological function*	*Distal steric hindrance*	*Proximal strain, weak Fe-His bond*	*Proximal His orientation*	*Distal site H-bond donor*	*Multiple-step NO binding*
sGC	NO sensor	No[a]	Strong[a]	ND[b]	No	Yes[c]
Cyt c′	NO sensor?[d]	Strong	No	Staggered[e]	No	Yes[c]
NS H-NOX	NO (redox?[d]) sensor	Moderate	No	Staggered	Weak	Yes[f]
Mb(II)	O_2 storage	Weak	Moderate	Eclipsed	Strong	No
Fe(II)PP(1-MeIm)	None, 5c Model Heme	No	No	Flexible[g]	No	No

[a]Most "Yes" or "No" are on the relative scale to indicate the major and minor factors.
[b]ND means three-dimensional structural information unavailable.
[c]The second [NO]-dependent binding is conversion from 6c to 5c-NO complex.
[d]"?" indicates possible but not proved function.
[e]Indicates the imidazole ring orientation relative to the pyrrole nitrogens (Fig. 7b).
[f]The second [NO]-dependent binding is the conversion from one 6c to another 6c-NO complex.
[g]A mixture of orientations due to absence of protein structure to achieve a rigid ring orientation.

His bond when NO is bound (123). At higher NO:heme ratios, a proximal 5c NO-heme complex is formed in a second bimolecular process, which depends on [NO] (species D in Fig. 8) (123, 131). As in the case of NO binding to cyt c′, a *bis*-NO complex is proposed as a transient intermediate at excess NO (species C in Fig. 8). Although this very transient species has not been verified by direct spectroscopic identification, its formation is strongly supported by the observed linear [NO]-dependence of the rate of 2nd step to form the final equilibrium 5c complex. In addition, our recent EPR freeze-trap study using ^{15}NO and ^{14}NO isotope ligands in sequential stopped-flow experiments confirms that heme iron coordinates the second NO molecule (123, 132). As in the case of cyt c′, the net result of the additional NO binding step is the generation of a high affinity 5c proximal heme-NO complex.

An alternative proposal is that the second NO is bound covalently to a cysteine thiol or at another nonheme site during the activation process (19, 32, 100–102). However, nitrosation of cysteine does not occur in the absence of O_2, and even in the presence of O_2, the association and dissociation reactions are too slow to contribute as an intermediate to the rapid formation of the final equilibrium 5c-NO complex with only one ligand bound (53, 69).

Complex mechanisms also appear to have evolved to allow *Ns* H-NOX and *CB* SONO, or *CB* H-NOX to have femptomolar K_D values for NO but only very weak or no O_2 binding under physiological conditions. In the case of *Ns* H-NOX, a multiple-step NO binding mechanism does occur, but the second [NO]-dependent step is a conversion from one type of 6c-NO complex (418 nm peak) to another (414 nm peak). The conversion from the 2nd 6c-NO complex to the final equilibrium 5c-NO complex is extremely slow, first order, and incomplete (122). The equilibrium 5c-NO complex formed for *CB* H-NOX is air stable, indicating that O_2 cannot readily displace the bound NO, as is also the case for sGC (81).

Physiological Importance of O_2 Exclusion and High NO Affinity

A summary of the mechanisms that have evolved to achieve O_2 discrimination and high NO affinity by a variety of heme proteins is given in Table 2 and based on the graphical analyses and kinetic parameters discussed in the previous sections of this review. While the biological functions of some of the other heme proteins are not certain, sGC behaves as a bona fide NO sensor. sGC requires high selectivity for NO over CO and complete exclusion of O_2 binding to prevent NO dioxygenation. The measured cellular level of NO in human embryonic kidney 293 T cells (HEK) cells, endothelial cells, and neuronal cells varies from picomolar to micromolar (11, 21, 128). Thus under normal conditions, the interaction between NO and sGC could occur at both high and sub-stoichiometric ratios.

Our recent study indicates that stoichiometric NO is still able to activate sGC to a level similar to that observed at excess NO, indicating that both 5c-NO complexes (D and D* in Fig. 8) may be capable of cyclase activation or that D* slowly isomerizes to D, even at low NO levels (123). The multi-step NO reaction with sGC leads to Fe-His bond breaking, formation of a 5c-NO complex with an apparent $K_D(NO)$ of $\sim 10^{-12}$ *M*, and generation of a protein conformation that is coupled to cyclase activation. Reversible CO binding to form a simple 6c CO-heme-His complex (A ↔ E in Fig. 8) does not appear to strongly activate sGC. The critical proximal strain that results in formation of the active 5c NO-heme complex also evolved to drastically reduce the affinity of sGC for O_2.

Exclusion of O_2 binding inhibits oxidation of the reduced heme iron to its inactive ferric form with simultaneous production of superoxide and, more importantly, prevents rapid dioxygenation of NO by bound O_2 to form biologically inactive nitrate. All heme proteins that reversibly bind O_2 also rapidly dioxygenate NO (35, 82). Thus, exclusion of O_2 by sGC is required for sensing low levels NO under aerobic conditions. This need for stringent ligand selectivity must be considered in searching for the biological functions for the other heme sensors, including cyt c′, *Ns* H-NOX, *CB* H-NOX, *etc.*, where NO sensing may need to occur at markedly different levels of O_2, particularly in the photosynthetic microorganisms.

Acknowledgments

We thank Elena Bogatenkova for expression and purification of $\alpha\beta$I145YsGC for ligand binding studies. This work was supported by U.S. Public Health Service Grants HL088128 (E.M.), HL095820 (A.-L.T.), GM35649 (J.S.O.), HL47020 (J.S.O.), American Heart Association, South Central Affiliate

Grant-in-Aid 09GRNT2060182] (E.M.), and Robert A. Welch Foundation Grant C0612 (J.S.O.).

References

1. Akimoto S, Tanaka A, Nakamura K, Shiro Y, and Nakamura H. O_2-specific regulation of the ferrous heme-based sensor kinase FixL from *Sinorhizobium meliloti* and its aberrant inactivation in the ferric form. *Biochem Biophys Res Commun* 304: 136–142, 2003.
2. Andrew CR, George SJ, Lawson DM, and Eady RR. Six- to five-coordinate heme-nitrosyl conversion in cytochrome c′ and its relevance to guanylate cyclase. *Biochemistry* 41: 2353–2360, 2002.
3. Andrew CR, Green EL, Lawson DM, and Eady RR. Resonance Raman studies of cytochrome c′ support the binding of NO and CO to opposite sides of the heme: implications for ligand discrimination in heme-based sensors. *Biochemistry* 40: 4115–4122, 2001.
4. Andrew CR, Kemper LJ, Busche TL, Tiwari AM, Kecskes MC, Stafford JM, Croft LC, Lu S, Moenne-Loccoz P, Huston W, Moir JW, and Eady RR. Accessibility of the distal heme face, rather than Fe-His bond strength, determines the heme-nitrosyl coordination number of cytochromes c′: evidence from spectroscopic studies. *Biochemistry* 44: 8664–8672, 2005.
5. Andrew CR, Rodgers KR, and Eady RR. A novel kinetic trap for NO release from cytochrome c′: a possible mechanism for NO release from activated soluble guanylate cyclase. *J Am Chem Soc* 125: 9548–9549, 2003.
6. Antonyuk SV, Rustage N, Petersen CA, Arnst JL, Heyes DJ, Sharma R, Berry NG, Scrutton NS, Eady RR, Andrew CR, and Hasnain SS. Carbon monoxide poisoning is prevented by the energy costs of conformational changes in gas-binding haemproteins. *Proc Natl Acad Sci U S A* 108: 15780–15785, 2011.
7. Aono S. Biochemical and biophysical properties of the CO-sensing transcriptional activator CooA. *Acc Chem Res* 36: 825–831, 2003.
8. Aono S, Honma Y, Ohkubo K, Tawara T, Kamiya T, and Nakajima H. CO sensing and regulation of gene expression by the transcriptional activator CooA. *J Inorg Biochem* 82: 51–56, 2000.
9. Aono S, Ohkubo K, Matsuo T, and Nakajima H. Redox-controlled ligand exchange of the heme in the CO-sensing transcriptional activator CooA. *J Biol Chem* 273: 25757–25764, 1998.
10. Balland V, Bouzhir-Sima L, Kiger L, Marden MC, Vos MH, Liebl U, and Mattioli TA. Role of arginine 220 in the oxygen sensor FixL from *Bradyrhizobium japonicum*. *J Biol Chem* 280: 15279–15288, 2005.
11. Batchelor AM, Bartus K, Reynell C, Constantinou S, Halvey EJ, Held KF, Dostmann WR, Vernon J, and Garthwaite J. Exquisite sensitivity to subsecond, picomolar nitric oxide transients conferred on cells by guanylyl cyclase-coupled receptors. *Proc Natl Acad Sci U S A* 107: 22060–22065, 2010.
12. Birukou I, Maillett DH, Birukova A, and Olson JS. Modulating distal cavities in the alpha and beta subunits of human HbA reveals the primary ligand migration pathway. *Biochemistry* 50: 7361–7374, 2011.
13. Boon EM, Huang SH, and Marletta MA. A molecular basis for NO selectivity in soluble guanylate cyclase. *Nat Chem Biol* 1: 53–59, 2005.
14. Boon EM and Marletta MA. Ligand discrimination in soluble guanylate cyclase and the H-NOX family of heme sensor proteins. *Curr Opin Chem Biol* 9: 441–446, 2005.
15. Boon EM and Marletta MA. Ligand specificity of H-NOX domains: from sGC to bacterial NO sensors. *J Inorg Biochem* 99: 892–902, 2005.
16. Bossa C, Amadei A, Daidone I, Anselmi M, Vallone B, Brunori M, and Di Nola A. Molecular dynamics simulation of sperm whale myoglobin: effects of mutations and trapped CO on the structure and dynamics of cavities. *Biophys J* 89: 465–474, 2005.
17. Burstyn JN, Yu AE, Dierks EA, Hawkins BK, and Dawson JH. Studies of the heme coordination and ligand binding properties of soluble guanylyl cyclase (sGC): characterization of Fe(II)sGC and Fe(II)sGC(CO) by electronic absorption and magnetic circular dichroism spectroscopies and failure of CO to activate the enzyme. *Biochemistry* 34: 5896–5903, 1995.
18. Carver TE, Brantley RE Jr., Singleton EW, Arduini RM, Quillin ML, Phillips GN Jr., and Olson JS. A novel site-directed mutant of myoglobin with an unusually high O_2 affinity and low autooxidation rate. *J Biol Chem* 267: 14443–14450, 1992.
19. Cary SP, Winger JA, Derbyshire ER, and Marletta MA. Nitric oxide signaling: no longer simply on or off. *Trends Biochem Sci* 31: 231–239, 2006.
20. Chang CK and Traylor TG. Reversible oxygenation of protoheme-imidazole complex in aqueous solution (1, 2). *Biochem Biophys Res Commun* 62: 729–735, 1975.
21. Chen K and Popel AS. Theoretical analysis of biochemical pathways of nitric oxide release from vascular endothelial cells. *Free Radic Biol Med* 41: 668–680, 2006.
22. Choi PS, Grigoryants VM, Abruna HD, Scholes CP, and Shapleigh JP. Regulation and function of cytochrome c′ in Rhodobacter sphaeroides 2.4.3. *J Bacteriol* 187: 4077–4085, 2005.
23. Choi S and Spiro TG. Out-of-plane deformation modes in the resonance Raman spectra of metalloporphyrins and heme proteins. *J Am Chem Soc* 105: 3683–3692, 1983.
24. Coyle CM, Vogel KM, Rush TS 3rd, Kozlowski PM, Williams R, Spiro TG, Dou Y, Ikeda-Saito M, Olson JS, and Zgierski MZ. FeNO structure in distal pocket mutants of myoglobin based on resonance Raman spectroscopy. *Biochemistry* 42: 4896–4903, 2003.
25. Deinum G, Stone JR, Babcock GT, and Marletta MA. Binding of nitric oxide and carbon monoxide to soluble guanylate cyclase as observed with Resonance raman spectroscopy. *Biochemistry* 35: 1540–1547, 1996.
26. Denninger JW and Marletta MA. Guanylate cyclase and the. NO/cGMP signaling pathway. *Biochim Biophys Acta* 1411: 334–350, 1999.
27. Denninger JW, Schelvis JP, Brandish PE, Zhao Y, Babcock GT, and Marletta MA. Interaction of soluble guanylate cyclase with YC-1: kinetic and resonance Raman studies. *Biochemistry* 39: 4191–4198, 2000.
28. Derbyshire ER, Gunn A, Ibrahim M, Spiro TG, Britt RD, and Marletta MA. Characterization of two different five-coordinate soluble guanylate cyclase ferrous-nitrosyl complexes. *Biochemistry* 47: 3892–3899, 2008.
29. Dioum EM, Rutter J, Tuckerman JR, Gonzalez G, Gilles-Gonzalez MA, and McKnight SL. NPAS2: a gas-responsive transcription factor. *Science* 298: 2385–2387, 2002.
30. Draghi F, Miele AE, Travaglini-Allocatelli C, Vallone B, Brunori M, Gibson QH, and Olson JS. Controlling ligand

binding in myoglobin by mutagenesis. *J Biol Chem* 277: 7509–7519, 2002.
31. Enemark JH and Feltham RD. Principles of structure, bonding, and reactivity for metal nitrosyl complexes. *Coord Chem Rev* 13: 339–406, 1974.
32. Fernhoff NB, Derbyshire ER, and Marletta MA. A nitric oxide/cysteine interaction mediates the activation of soluble guanylate cyclase. *Proc Natl Acad Sci U S A* 106: 21602–21607, 2009.
33. Franzen S. Spin-dependent mechanism for diatomic ligand binding to heme. *Proc Natl Acad Sci U S A* 99: 16754–16759, 2002.
34. Fritz BG, Hu X, Brailey JL, Berry RE, Walker FA, and Montfort WR. Oxidation and loss of heme in soluble guanylyl cyclase from *Manduca sexta*. *Biochemistry* 50: 5813–5815, 2011.
35. Gardner PR, Gardner AM, Brashear WT, Suzuki T, Hvitved AN, Setchell KD, and Olson JS. Hemoglobins dioxygenate nitric oxide with high fidelity. *J Inorg Biochem* 100: 542–550, 2006.
36. Garton EM, Pixton DA, Petersen CA, Eady RR, Hasnain SS, and Andrew CR. A distal pocket leu residue inhibits the binding of O(2) and NO at the distal heme site of cytochrome c′. *J Am Chem Soc* 134: 1461–1463, 2012.
37. George SJ, Andrew CR, Lawson DM, Thorneley RN, and Eady RR. Stopped-flow infrared spectroscopy reveals a six-coordinate intermediate in the formation of the proximally bound five-coordinate NO adduct of cytochrome c′. *J Am Chem Soc* 123: 9683–9684, 2001.
38. Giangiacomo L, Ilari A, Boffi A, Morea V, and Chiancone E. The truncated oxygen-avid hemoglobin from *Bacillus subtilis*: X-ray structure and ligand binding properties. *J Biol Chem* 280: 9192–9202, 2005.
39. Gilles-Gonzalez MA and Gonzalez G. Heme-based sensors: defining characteristics, recent developments, and regulatory hypotheses. *J Inorg Biochem* 99: 1–22, 2005.
40. Gonzalez G, Dioum EM, Bertolucci CM, Tomita T, Ikeda-Saito M, Cheesman MR, Watmough NJ, and Gilles-Gonzalez MA. Nature of the displaceable heme-axial residue in the EcDos protein, a heme-based sensor from *Escherichia coli*. *Biochemistry* 41: 8414–8421, 2002.
41. Hargrove MS, Barry JK, Brucker EA, Berry MB, Phillips GN Jr., Olson JS, Arredondo-Peter R, Dean JM, Klucas RV, and Sarath G. Characterization of recombinant soybean leghemoglobin a and apolar distal histidine mutants. *J Mol Biol* 266: 1032–1042, 1997.
42. Hoshino M, Ozawa, K, Seki H, and Ford PC. Photochemistry of nitric oxide adducts of water-soluble iron(III) porphyrin and ferrihemoproteins studied by nanosecond laser photolysis. *J Am Chem Soc* 115: 9568–9575, 1993.
43. Hough MA, Antonyuk SV, Barbieri S, Rustage N, McKay AL, Servid AE, Eady RR, Andrew CR, and Hasnain SS. Distal-to-proximal NO conversion in hemoproteins: the role of the proximal pocket. *J Mol Biol* 405: 395–409, 2011.
44. Ignarro LJ. Heme-dependent activation of soluble guanylate cyclase by nitric oxide: regulation of enzyme activity by porphyrins and metalloporphyrins. *Semin Hematol* 26: 63–76, 1989.
45. Ilari A, Bonamore A, Farina A, Johnson KA, and Boffi A. The X-ray structure of ferric *Escherichia coli* flavohemoglobin reveals an unexpected geometry of the distal heme pocket. *J Biol Chem* 277: 23725–23732, 2002.
46. Ionascu D, Gruia F, Ye X, Yu A, Rosca F, Beck C, Demidov A, Olson JS, and Champion PM. Temperature-dependent studies of NO recombination to heme and heme proteins. *J Am Chem Soc* 127: 16921–16934, 2005.
47. Jain R and Chan MK. Mechanisms of ligand discrimination by heme proteins. *J Biol Inorg Chem* 8: 1–11, 2003.
48. Karow DS, Pan D, Tran R, Pellicena P, Presley A, Mathies RA, and Marletta MA. Spectroscopic characterization of the soluble guanylate cyclase-like heme domains from *Vibrio cholerae* and *Thermoanaerobacter tengcongensis*. *Biochemistry* 43: 10203–10211, 2004.
49. Kassner RJ. Ligand binding properties of cytochromes c′. *Biochim Biophys Acta* 1058: 8–12, 1991.
50. Kassner RJ, Kykta MG, and Cusanovich MA. Binding of cyanide to cytochrome c′ from *Chromatium vinosum*. *Biochim Biophys Acta* 831: 155–158, 1985.
51. Kharitonov VG, Russwurm M, Magde D, Sharma VS, and Koesling D. Dissociation of nitric oxide from soluble guanylate cyclase. *Biochem Biophys Res Commun* 239: 284–286, 1997.
52. Kharitonov VG, Sharma VS, Magde D, and Koesling D. Kinetics of nitric oxide dissociation from five- and six-coordinate nitrosyl hemes and heme proteins, including soluble guanylate cyclase. *Biochemistry* 36: 6814–6818, 1997.
53. Kharitonov VG, Sundquist AR, and Sharma VS. Kinetics of nitrosation of thiols by nitric oxide in the presence of oxygen. *J Biol Chem* 270: 28158–28164, 1995.
54. Koesling D, Bohme E, and Schultz G. Guanylyl cyclases, a growing family of signal-transducing enzymes. *FASEB J* 5: 2785–2791, 1991.
55. Kruglik SG, Lambry JC, Cianetti S, Martin JL, Eady RR, Andrew CR, and Negrerie M. Molecular basis for nitric oxide dynamics and affinity with *Alcaligenes xylosoxidans* cytochrome c. *J Biol Chem* 282: 5053–5062, 2007.
56. Kundu S and Hargrove MS. Distal heme pocket regulation of ligand binding and stability in soybean leghemoglobin. *Proteins* 50: 239–248, 2003.
57. Kundu S, Snyder B, Das K, Chowdhury P, Park J, Petrich JW, and Hargrove MS. The leghemoglobin proximal heme pocket directs oxygen dissociation and stabilizes bound heme. *Proteins* 46: 268–277, 2002.
58. Kurokawa H, Lee DS, Watanabe M, Sagami I, Mikami B, Raman CS, and Shimizu T. A redox-controlled molecular switch revealed by the crystal structure of a bacterial heme PAS sensor. *J Biol Chem* 279: 20186–20193, 2004.
59. Lawson DM, Stevenson CE, Andrew CR, and Eady RR. Unprecedented proximal binding of nitric oxide to heme: implications for guanylate cyclase. *EMBO J* 19: 5661–5671, 2000.
60. Li T, Quillin ML, Phillips GN Jr., and Olson JS. Structural determinants of the stretching frequency of CO bound to myoglobin. *Biochemistry* 33: 1433–1446, 1994.
61. Linder DP, Rodgers KR, Banister J, Wyllie GR, Ellison MK, and Scheidt WR. Five-coordinate Fe(III)NO and Fe(II)CO porphyrinates: where are the electrons and why does it matter? *J Am Chem Soc* 126: 14136–14148, 2004.
62. Lou BS, Snyder JK, Marshall P, Wang JS, Wu G, Kulmacz RJ, Tsai AL, and Wang J. Resonance Raman studies indicate a unique heme active site in prostaglandin H synthase. *Biochemistry* 39: 12424–12434, 2000.
63. Ma X, Sayed N, Beuve A, and van den Akker F. NO and CO differentially activate soluble guanylyl cyclase via a heme pivot-bend mechanism. *EMBO J* 26: 578–588, 2007.
64. Makino R, Matsuda H, Obayashi E, Shiro Y, Iizuka T, and Hori H. EPR characterization of axial bond in metal center

of native and cobalt-substituted guanylate cyclase. *J Biol Chem* 274: 7714–7723, 1999.
65. Makino R, Park SY, Obayashi E, Iizuka T, Hori H, and Shiro Y. Oxygen binding and redox properties of the heme in soluble guanylate cyclase: implications for the mechanism of ligand discrimination. *J Biol Chem* 286: 15678–15687, 2011.
66. Marletta MA. Nitric oxide: biosynthesis and biological significance. *Trends Biochem Sci* 14: 488–492, 1989.
67. Marti MA, Capece L, Crespo A, Doctorovich F, and Estrin DA. Nitric oxide interaction with cytochrome c′ and its relevance to guanylate cyclase. Why does the iron histidine bond break? *J Am Chem Soc* 127: 7721–7728, 2005.
68. Martin E, Berka V, Bogatenkova E, Murad F, and Tsai AL. Ligand selectivity of soluble guanylyl cyclase: effect of the hydrogen bonding tyrosine in the distal heme pocket on binding of oxygen, nitric oxide and carbon monoxide. *J Biol Chem* 281: 27836–27845, 2006.
69. Martin E, Berka V, Tsai A-L, and Murad F. Soluble guanylyl cyclase: the nitric oxide receptor. *Methods Enzymol* 396: 478–492, 2005.
70. Mathews AJ, Rohlfs RJ, Olson JS, Tame J, Renaud JP, and Nagai K. The effects of E7 and E11 mutations on the kinetics of ligand binding to R state human hemoglobin. *J Biol Chem* 264: 16573–16583, 1989.
71. Mayburd AL and Kassner RJ. Mechanism and biological role of nitric oxide binding to cytochrome c′. *Biochemistry* 41: 11582–11591, 2002.
72. McCleverty JA. Chemistry of nitric oxide relevant to biology. *Chem Rev* 104: 403–418, 2004.
73. Miele AE, Santanche S, Travaglini-Allocatelli C, Vallone B, Brunori M, and Bellelli A. Modulation of ligand binding in engineered human hemoglobin distal pocket. *J Mol Biol* 290: 515–524, 1999.
74. Monson EK, Weinstein M, Ditta GS, and Helinski DR. The FixL protein of *Rhizobium meliloti* can be separated into a heme-binding oxygen-sensing domain and a functional C-terminal kinase domain. *Proc Natl Acad Sci U S A* 89: 4280–4284, 1992.
75. Motie M, Kassner RJ, Meyer TE, and Cusanovich MA. Kinetics of cyanide binding to *Chromatium vinosum* ferricytochrome c′. *Biochemistry* 29: 1932–1936, 1990.
76. Mukai M, Ouellet Y, Ouellet H, Guertin M, and Yeh SR. NO binding induced conformational changes in a truncated hemoglobin from *Mycobacterium tuberculosis*. *Biochemistry* 43: 2764–2770, 2004.
77. Mukai M, Savard PY, Ouellet H, Guertin M, and Yeh SR. Unique ligand-protein interactions in a new truncated hemoglobin from *Mycobacterium tuberculosis*. *Biochemistry* 41: 3897–3905, 2002.
78. Murad F, Arnold WP, Mittal CK, and Braughler JM. Properties and regulation of guanylate cyclase and some proposed functions for cyclic GMP. *Adv Cyclic Nucleotide Res* 11: 175–204, 1979.
79. Nagai K and Kitagawa T. Differences in Fe(II)-N epsilon (His-F8) stretching frequencies between deoxyhemoglobins in the two alternative quaternary structures. *Proc Natl Acad Sci U S A* 77: 2033–2037, 1980.
80. Nagai K, Luisi B, Shih D, Miyazaki G, Imai K, Poyart C, De Young A, Kwiatkowsky L, Noble RW, Lin SH, *et al*. Distal residues in the oxygen binding site of haemoglobin studied by protein engineering. *Nature* 329: 858–860, 1987.
81. Nioche P, Berka V, Vipond J, Minton N, Tsai A-L, and Raman CS. Femtomolar sensitivity of a NO sensor from *Clostridium botulinum*. *Science* 306: 1550–1553, 2004.
82. Olson JS, Foley EW, Rogge C, Tsai A-L, Doyle MP, and Lemon DD. No scavenging and the hypertensive effect of hemoglobin-based blood substitutes. *Free Radic Biol Med* 36: 685–697, 2004.
83. Olson JS and Phillips GN Jr. Kinetic pathways and barriers for ligand binding to myoglobin. *J Biol Chem* 271: 17596, 1996.
84. Olson JS and Phillips GNJ. Myoglobin discriminates between O_2, NO, and CO by electrostatic interactions with the bound ligand. *J Biol Inorg Chem* 2: 544–552, 1997.
85. Olson JS, Rohlfs RJ, and Gibson QH. Ligand recombination to the alpha and beta subunits of human hemoglobin. *J Biol Chem* 262: 12930–12938, 1987.
86. Olson JS, Soman J, and Phillips GN Jr. Ligand pathways in myoglobin: a review of Trp cavity mutations. *IUBMB Life* 59: 552–562, 2007.
87. Pellicena P, Karow DS, Boon EM, Marletta MA, and Kuriyan J. Crystal structure of an oxygen-binding heme domain related to soluble guanylate cyclases. *Proc Natl Acad Sci U S A* 101: 12854–12859, 2004.
88. Pesce A, Nardini M, Ascenzi P, Geuens E, Dewilde S, Moens L, Bolognesi M, Riggs AF, Hale A, Deng P, Nienhaus GU, Olson JS, and Nienhaus K. Thr-E11 regulates O_2 affinity in *Cerebratulus lacteus* mini-hemoglobin. *J Biol Chem* 279: 33662–33672, 2004.
89. Peterson ES, Huang S, Wang J, Miller LM, Vidugiris G, Kloek AP, Goldberg DE, Chance MR, Wittenberg JB, and Friedman JM. A comparison of functional and structural consequences of the tyrosine B10 and glutamine E7 motifs in two invertebrate hemoglobins (*Ascaris suum* and *Lucina pectinata*). *Biochemistry* 36: 13110–13121, 1997.
90. Phillips GN Jr., Teodoro ML, Li T, Smith B, and Olson JS. Bound CO is a molecular probe of electrostatic potential in the distal pocket of myoglobin. *J Phys Chem B* 103: 8817–8829, 1999.
91. Poulos TL. Soluble guanylate cyclase. *Curr Opin Struct Biol* 16: 736–743, 2006.
92. Quillin ML, Arduini RM, Olson JS, and Phillips GN Jr. High-resolution crystal structures of distal histidine mutants of sperm whale myoglobin. *J Mol Biol* 234: 140–155, 1993.
93. Quillin ML, Li T, Olson JS, Phillips GN Jr., Dou Y, Ikeda-Saito M, Regan R, Carlson M, Gibson QH, Li H, *et al.* Structural and functional effects of apolar mutations of the distal valine in myoglobin. *J Mol Biol* 245: 416–436, 1995.
94. Reynolds MF, Parks RB, Burstyn JN, Shelver D, Thorsteinsson MV, Kerby RL, Roberts GP, Vogel KM, and Spiro TG. Electronic absorption, EPR, and resonance Raman spectroscopy of CooA, a CO-sensing transcription activator from *R. rubrum*, reveals a five-coordinate NO-heme. *Biochemistry* 39: 388–396, 2000.
95. Roberts GP, Thorsteinsson MV, Kerby RL, Lanzilotta WN, and Poulos T. CooA: a heme-containing regulatory protein that serves as a specific sensor of both carbon monoxide and redox state. *Prog Nucleic Acid Res Mol Biol* 67: 35–63, 2001.
96. Roberts GP, Youn H, and Kerby RL. CO-sensing mechanisms. *Microbiol Mol Biol Rev* 68: 453–473, 2004.
97. Rodgers KR. Heme-based sensors in biological systems. *Curr Opin Chem Biol* 3: 158–167, 1999.
98. Rohlfs RJ, Mathews AJ, Carver TE, Olson JS, Springer BA, Egeberg KD, and Sligar SG. The effects of amino acid substitution at position E7 (residue 64) on the kinetics of ligand binding to sperm whale myoglobin. *J Biol Chem* 265: 3168–3176, 1990.
99. Rose EJ, Venkatasubramanian PN, Swartz JC, Jones RD, Basolo F, and Hoffman BM. Carbon monoxide binding

kinetics in "capped" porphyrin compounds. *Proc Natl Acad Sci U S A* 79: 5742–5745, 1982.
100. Russwurm M and Koesling D. Guanylyl cyclase: NO hits its target. *Biochem Soc Symp* 51–63, 2004.
101. Russwurm M and Koesling D. NO activation of guanylyl cyclase. *EMBO J* 23: 4443–4450, 2004.
102. Sayed N, Baskaran P, Ma X, van den Akker F, and Beuve A. Desensitization of soluble guanylyl cyclase, the NO receptor, by S-nitrosylation. *Proc Natl Acad Sci U S A* 104: 12312–12317, 2007.
103. Schlichting I, Berendzen J, Phillips GN Jr., and Sweet RM. Crystal structure of photolysed carbonmonoxy-myoglobin. *Nature* 371: 808–812, 1994.
104. Scott EE, Gibson QH, and Olson JS. Mapping the pathways for O_2 entry into and exit from myoglobin. *J Biol Chem* 276: 5177–5188, 2001.
105. Seibold SA, Cerda JF, Mulichak AM, Song I, Garavito RM, Arakawa T, Smith WL, and Babcock GT. Peroxidase activity in prostaglandin endoperoxide H synthase-1 occurs with a neutral histidine proximal heme ligand. *Biochemistry* 39: 6616–6624, 2000.
106. Sharma VS and Magde D. Activation of soluble guanylate cyclase by carbon monoxide and nitric oxide: a mechanistic model. *Methods* 19: 494–505, 1999.
107. Sharma VS, Traylor TG, Gardiner R, and Mizukami H. Reaction of nitric oxide with heme proteins and model compounds of hemoglobin. *Biochemistry* 26: 3837–3843, 1987.
108. Smerdon SJ, Dodson GG, Wilkinson AJ, Gibson QH, and Blackmore RS. Distal pocket polarity in ligand binding to myoglobin: structural and functional characterization of a threonine68(E11) mutant. *Biochemistry* 30: 6252–6260, 1991.
109. Soda K, Ohba Y, and Zaitsu K. Assay of human platelet guanylate cyclase activity by high-performance liquid chromatography with fluorescence derivatization. *J Chromatogr B Biomed Sci Appl* 752: 55–60, 2001.
110. Soldatova AV, Ibrahim M, Olson JS, Czernuszewicz RS, and Spiro TG. New light on NO bonding in Fe(III) heme proteins from resonance Raman spectroscopy and DFT modeling. *J Am Chem Soc* 132: 4614–4625, 2010.
111. Springer BA, Egeberg KD, Sligar SG, Rohlfs RJ, Mathews AJ, and Olson JS. Discrimination between oxygen and carbon monoxide and inhibition of autooxidation by myoglobin. Site-directed mutagenesis of the distal histidine. *J Biol Chem* 264: 3057–3060, 1989.
112. Stone JR and Marletta MA. The ferrous heme of soluble guanylate cyclase: formation of hexacoordinate complexes with carbon monoxide and nitrosomethane. *Biochemistry* 34: 16397–16403, 1995.
113. Stone JR and Marletta MA. Soluble guanylate cyclase from bovine lung: activation with nitric oxide and carbon monoxide and spectral characterization of the ferrous and ferric states. *Biochemistry* 33: 5636–5640, 1994.
114. Stone JR and Marletta MA. Spectral and kinetic studies on the activation of soluble guanylate cyclase by nitric oxide. *Biochemistry* 35: 1093–1099, 1996.
115. Stone JR, Sands RH, Dunham WR, and Marletta MA. Spectral and ligand-binding properties of an unusual hemoprotein, the ferric form of soluble guanylate cyclase. *Biochemistry* 35: 3258–3262, 1996.
116. Strickland N and Harvey JN. Spin-forbidden ligand binding to the ferrous-heme group: ab initio and DFT studies. *J Phys Chem B* 111: 841–852, 2007.
117. Tahirov TH, Misaki S, Meyer TE, Cusanovich MA, Higuchi Y, and Yasuoka N. High-resolution crystal structures of two polymorphs of cytochrome c′ from the purple phototrophic bacterium rhodobacter capsulatus. *J Mol Biol* 259: 467–479, 1996.
118. Tomita T, Gonzalez G, Chang AL, Ikeda-Saito M, and Gilles-Gonzalez MA. A comparative resonance Raman analysis of heme-binding PAS domains: heme iron coordination structures of the BjFixL, AxPDEA1, EcDos, and MtDos proteins. *Biochemistry* 41: 4819–4826, 2002.
119. Traylor TG and Sharma VS. Why NO? *Biochemistry* 31: 2847–2849, 1992.
120. Tsai A-L. How does NO activate hemeproteins? *FEBS Lett* 341: 141–145, 1994.
121. Tsai A-L, Berka V, Martin E, and Olson JS. A "sliding-scale rule" for selectivity between NO, CO and O_2 by heme protein sensors. *Biochemistry* 51: 172–186, 2012.
122. Tsai A-L, Berka V, Martin FE, Ma X, van den Akker F, Fabian M, and Olson JS. Is Nostoc H-NOX an NO sensor or redox switch? *Biochemistry* 49: 6587–6599, 2010.
123. Tsai A-L, Berka V, Sharina I, and Martin E. Dynamic ligand exchange in soluble guanylyl cyclase: implications for sGC regulation and desensitization. *J Biol Chem* 286: 43182–43192, 2011.
124. Unzai S, Eich R, Shibayama N, Olson JS, and Morimoto H. Rate constants for O_2 and CO binding to the alpha and beta subunits within the R and T states of human hemoglobin. *J Biol Chem* 273: 23150–23159, 1998.
125. Vojtechovsky J, Chu K, Berendzen J, Sweet RM, and Schlichting I. Crystal structures of myoglobin-ligand complexes at near-atomic resolution. *Biophys J* 77: 2153–2174, 1999.
126. Walker FA. Nitric oxide interaction with insect nitrophorins and thoughts on the electron configuration of the {FeNO}6 complex. *J Inorg Biochem* 99: 216–236, 2005.
127. Weichsel A, Andersen JF, Roberts SA, and Montfort WR. Nitric oxide binding to nitrophorin 4 induces complete distal pocket burial. *Nat Struct Biol* 7: 551–554, 2000.
128. Wood KC, Batchelor AM, Bartus K, Harris KL, Garthwaite G, Vernon J, and Garthwaite J. Picomolar nitric oxide signals from central neurons recorded using ultrasensitive detector cells. *J Biol Chem* 286: 43172–43181, 2011.
129. Yu NT. Resonance Raman studies of ligand binding. *Methods Enzymol* 130: 351–409, 1986.
130. Zhang W, Olson JS, and Phillips GN Jr. Biophysical and kinetic characterization of HemAT, an aerotaxis receptor from *Bacillus subtilis*. *Biophys J* 88: 2801–2814, 2005.
131. Zhao Y, Brandish PE, Ballou DP, and Marletta MA. A molecular basis for nitric oxide sensing by soluble guanylate cyclase. *Proc Natl Acad Sci U S A* 96: 14753–14758, 1999.
132. Martin E, Berka V, Sharina I, and Tsai A-L. Mechanism of NO binding to soluble guanylyl cyclase: implication for the second NO binding to the heme proximal site. Biochemistry 2012 (In press).

Address correspondence to:
Prof. Ah-lim Tsai
Division of Hematology
University of Texas Health Science Center at Houston
6431 Fannin St.
P.O. Box 20708
Houston, TX 77225

E-mail: ah-lim.tsai@uth.tmc.edu

Date of first submission to ARS Central, February 13, 2012; date of acceptance, February 18, 2012.

Abbreviations Used

5c-NO complex = five coordinate NO complex
6c-NO complex = six coordinate NO complex
AXCP cyt c′ = *Alcaligenes xylosoxidans* cytochrome c′
CB = *Clostridium botulinum*
CO = carbon monoxide
EPR = electron paramagnetic resonance
Fe(II) = ferrous heme
Fe(III) = ferric heme
Hb = hemoglobin
H-NOX = heme nitric oxide/oxygen-binding domain
I145Y sGC = sGC with site-specific replacement of isoleucine by a tyrosine on residue 145
L2 H-NOX = *Legionella pneumophila* H-NOX
Mb = myoglobin
NO = nitric oxide
Ns = *Nostoc puntiforme*
O_2 = dioxygen
PDB = Protein Data Bank
PGHS-1 = prostaglandin H synthase type 1
rR = resonance Raman spectroscopy
sGC = soluble guanylyl cyclase
SONO = sensor of NO
Tt = *Thermoanaerobacter tengcongensis*